Integrated Arctic Observation System

Research and Innovation Action under EC Horizon2020
Grant Agreement no. 727890

Project coordinator:
Nansen Environmental and Remote Sensing Center, Norway

Deliverable 6.4

Ice-ocean statistics and state estimation V1

Observing System Assimilation experiments in the Arctic Ocean and

A 10-year Arctic ocean-sea ice state estimation using the adjoint method

Authors: Guokun Lyu, Nuna Serra, Armin Koehl and Detlef Stammer

Version	DATE	CHANGE RECORDS	LEAD AUTHOR
1.0	24/02/2019	Template	LH Pettersson / K Lygre
1.1	08/01/2020	Draft	Guokun Lyu
1.2	28/01/2020	Final version; minor revisions	Guokun Lyu
1.3	04/02/2020	Review; technical review and submission	K Lygre

Approval X	Date: 4 February 2020	Sign. Coordinator

USED PERSON-MONTHS FOR THIS DELIVERABLE					
No	*Beneficiary*	*PM*	*No*	*Beneficiary*	*PM*
1	NERSC		24	TDUE	
2	UiB		25	GINR	
3	IMR		26	UNEXE	
4	MISU		27	NIVA	
5	AWI		28	CNRS	
6	IOPAN		29	U Helsinki	
7	DTU		30	GFZ	
8	AU		31	ARMINE	
9	GEUS		32	IGPAN	
10	FMI		33	U SLASKI	
11	UNIS		34	BSC	
12	NORDECO		35	DNV GL	
13	SMHI		36	RIHMI-WDC	
14	USFD		37	NIERSC	
15	NUIM		38	WHOI	
16	IFREMER		39	SIO	
17	MPG		40	UAF	
18	EUROGOOS		41	U Laval	
19	EUROCEAN		42	ONC	
20	UPM		43	NMEFC	
21	UB		44	RADI	
22	UHAM	*13*	45	KOPRI	
23	NORUT		46	NIPR	
			47	PRIC	

DISSEMINATION LEVEL		
PU	Public, fully open	X
CO	Confidential, restricted under conditions set out in Model Grant Agreement	
CI	Classified, information as referred to in Commission Decision 2001/844/EC	

EXECUTIVE SUMMARY

Based on a coupled ocean-sea ice model and its adjoint model, we evaluate the capacity of the existing Arctic Ocean observing system on capturing different aspects of the Arctic Ocean changes, using Observing System Simulation Experiments (OSSEs). Subsequently, we produce a 10-year ocean-sea ice synthesis by assimilating all available observations into the system.

The main finds are:

1) Moorings deployed in the Fram Strait and along the pathway of Atlantic inflow to the Arctic Ocean are critical to capture the remote-propagating signals. The existing mooring system needs to be enhanced.
2) Sea ice processes, especially sea ice concentration changes, are the dominant mode that is improved by data assimilation. The improvement benefits from the spatiotemporal coverage of sea ice concentration observations.
3) Changes in the temperature and salinity are tiny in the ice-covered region and are caused by enhanced air-sea interaction due to sea ice reduction. Although the availability of hydrographic profiles increased significantly over the past decades, its effects are not apparent in the data assimilation experiments.

Table of Contents

1. Introduction

The Arctic Ocean plays a critical role in warming the earth system due to the existence of sea ice and the large freshwater storage. Model studies (Köhl & Serra, 2014; Proshutinsky & Johnson, 1997) suggested that the storage and the release of freshwater are related to basin-wide cyclonic/anti-cyclonic ocean circulation anomalies caused by Arctic Oscillation. The releasing of freshwater to the Atlantic Ocean modulates deep-water formation and therefore changes the Atlantic meridional Circulation (Jungclaus et al., 2005). Over the past two decades, observations demonstrate that the Arctic Ocean experiences rapid changes with increased freshwater storage (Proshutinsky et al., 2009), increased sea level (Armitage et al., 2016; Rose et al., 2019), increased ocean mass (Morison et al., 2007), reduced ice cap (Comiso et al., 2008; Kwok & Rothrock, 2009), and enhanced inflow from the Atlantic Ocean (Woodgate et al., 2012) and the Pacific Ocean (Dmitrenko et al., 2008; Quadfasel et al., 1991). Recent studies based on observations and models (Dukhovskoy et al., 2004; Giles et al., 2012; Morison et al., 2012; Polyakov et al., 2010; Zhang & Steele, 2007) improved our understanding of interactions between different aspects of the Arctic Ocean. However, neither models nor observations have revealed a complete picture of the Arctic Ocean changes, especially the interactions between different aspects of the Arctic system, due to the lack of observations and model deficiencies (Jahn et al., 2012; Proshutinsky et al., 2011).

Understanding the complex processes of the Arctic system is critical for predicting its changes in the warming earth and for evaluating its impacts on the other components of the earth system. Despite recent improvements in the observing capability of the Arctic Ocean, the Arctic Ocean remains one of the least observed areas of the global ocean. This situation is mainly caused by the harsh operating conditions and by diplomatic constraints requiring that individual observing system components are deployed uncoordinated between nations. Attempts are being made now to integrate those different components into one sustainable and long-term Pan-Arctic observing system with improved temporal and spatial observing coverages, which could better monitor changes across the entire Arctic basin. On the other hand, data assimilation techniques have been applied to assimilate available observations into state-of-the-art coupled ocean-sea ice models, producing ocean reanalysis for better understanding dynamic processes (see Uotila et al., 2019). Improvements in different aspects of the simulated Arctic marine parameters are found in the reanalysis datasets (e.g., Koldunov et al., 2017; Xie et al., 2017). Discrepancies among different reanalysis are assessed, which may relate to different models, various data assimilation techniques, and observations assimilated. However, most of the Arctic reanalysis products are based on operational forecast systems and suffer from imbalance due to adjustment of the initial condition periodically (usually 1~7 days).

A better option for the ocean synthesis could be the adjoint method with a long assimilation window (e.g., Koldunov et al., 2017), which produces a synthesis product that is dynamically consistent with the model dynamics. Despite the application of data assimilation techniques in the Arctic Ocean, it remains unclear the potential effects of existing observing systems on improving different aspects of the Arctic Ocean due to the lack of independent observations. In this study, we will further apply the adjoint method to assimilate observations into a coupled ocean-sea ice model.

This study has two goals:

1) Assessing the impacts of Observing System on Monitoring the Arctic Ocean Changes using Observing System Simulating Experiments (OSSEs).

2) Assimilate all available observations into the model to produce an Arctic Ocean synthesis from the year 2007-2016.

The structure of the remaining report is as follows: In section 2, we introduce the coupled ocean-sea ice data assimilation system and the Arctic Ocean observing systems. Analysis of OSSEs and the effects of individual observing systems are in section 3. In section 4, we introduce the 10-year Arctic ocean-sea ice synthesis. And section 5 summarises the results in both the OSSEs and the 10-year ocean-sea ice synthesis.

2. Data Assimilation System and Observations

The data assimilation system is based on the framework of the Estimating the Circulation and Climate of the Ocean consortium (ECCO), specifically the work of Fenty and Heimbach (2013), using the MIT ocean general circulation model (Marshall et al., 1997) and its adjoint model generated by the Transformation of Algorithms in Fortran (TAF, Giering & Kaminski, 1998). Applications of this system to adjoint sensitivity analysis and ocean-sea ice reanalysis are reported in Koldunov et al. (2013) and Koldunov et al. (2017). Here, the model setup, data assimilation method, and the Arctic Ocean observing systems are described below.
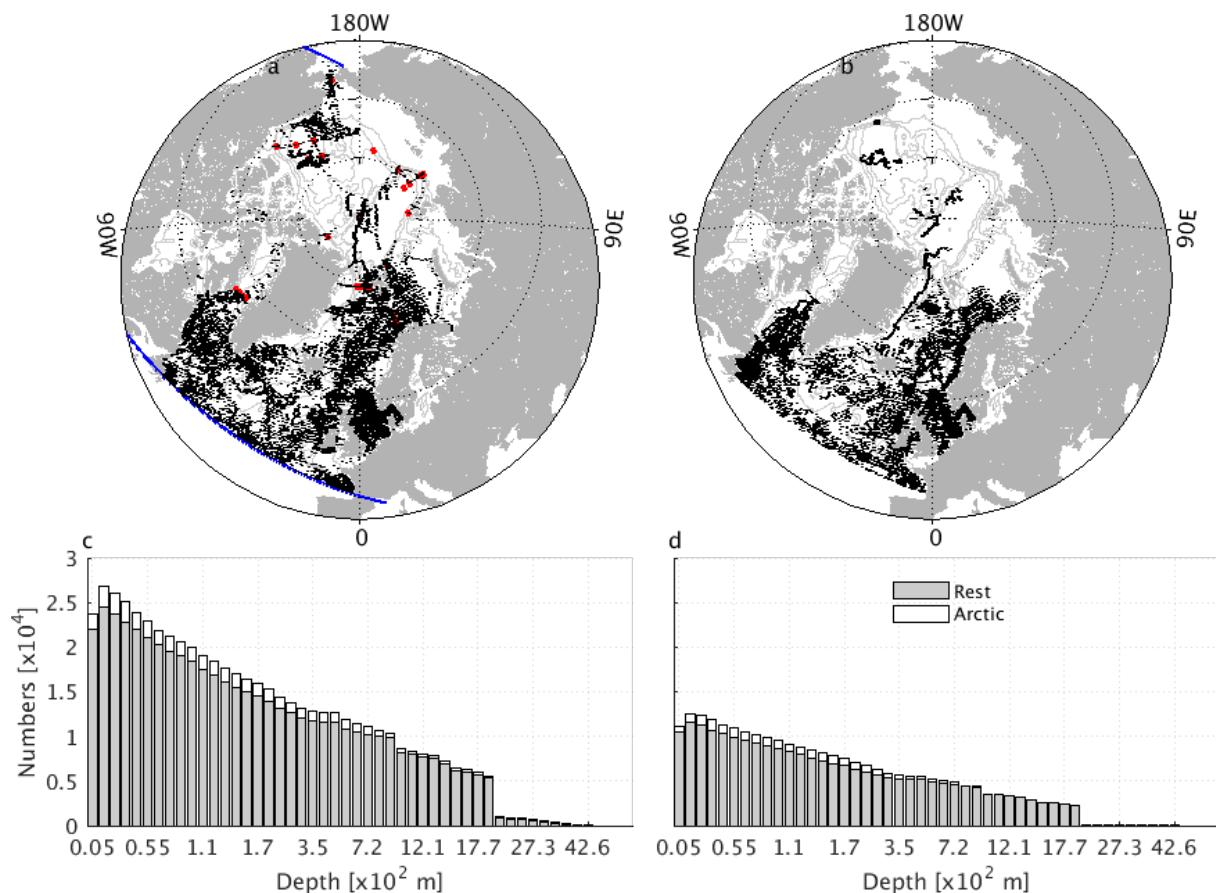
Figure 1. Model domain (enclosed by the blue line in a), distribution of hydrographic profiles in the summertime (May-October, black dots in a) and wintertime (November-April, black dots in b). The red dots mark locations of the moorings deployed in the Davis Strait, the Bering Strait, the Fram Strait, the Barents Sea Opening, and by the Nansen and Amundsen Basins Observational System (NABOS), the North Pole Environmental Observatory (NPEO), and the Beaufort Gyre Exploration Project (BGEP) project. Panels c and d show the number of observations within the Arctic Ocean (white bars) and the rest of the model domain (grey bars) in the summer season (c) and the winter season (d), depending on depth.

2.1 Model setup

The model domain of the data assimilation system covers the entire Arctic Ocean north of the Bering Strait and the Atlantic Ocean north of ~44°N (blue lines in Figure 1a). It uses a curvilinear grid with a horizontal resolution ~16 km. In the vertical, the simulation use z-coordinate and has 50 levels, with a resolution ranging from 10 m in the surface to ~456 m in the deep ocean. The bathymetry is derived from ETOPO2 datasets (Smith & Sandwell, 1997).

At the ocean surface, bulk formulae and atmospheric state from the 6-hourly NCEP RE1 (Kalnay et al., 1996), including 2 m air temperature, 2 m specific humidity, precipitation rate, 10 m wind vectors, downward longwave radiation, and net shortwave radiation, are used to compute the momentum, freshwater, and heat fluxes. At the southern and northern open boundaries, the model is forced by the monthly output from an 8-km Atlantic-Arctic simulation (Koldunov et al., 2014). At the river mouths, a seasonally varying river runoff is applied. A virtual salt flux parameterization is used to mimic the effect of freshwater input/output on salinity, and a K-profile parameterization scheme of Large et al. (1994) is adopted to parameterize the unresolved mixing processes. A dynamic-thermodynamic sea ice model is used to predict sea ice concentration, ice thickness, and ice velocity. The thermodynamic component is a variation of zero-layer formation of Semtner (1976), and the dynamic component is based on (Hibler III, 1979, 1980) and implemented following the work of Zhang and Hibler III (1997). The sea ice submodel is then evolved (Losch et al., 2010) and improved for the application of synthesis with the adjoint method (Fenty & Heimbach, 2013).

In OSSEs, a nature run is required to generate pseudo-observations. In this study, a 4-km Atlantic-Arctic simulation based on MITgcm is used. Configuration of this 4-km Atlantic-Arctic simulation is similar to the assimilation model above except that: 1) the nature run has a higher horizontal (~4 km) and vertical (100 levels) resolutions; 2) it use ERA-Interim (Dee et al., 2011) reanalysis as surfacing forcing; 3) it cover the entire Arctic Ocean north of Bering Strait and the Atlantic Ocean north of 33°S.

2.2 The Adjoint Data Assimilation Approach

We use an adjoint method to assimilate observations into our coupled ocean-sea ice model. This method brings model simulation into consistency with available observations by minimizing a cost function through adjusting the control variables (the initial state and atmospheric forcing in this study) within a long assimilation window.

Formally, a quadric form cost function is defined as,

$$J(C_{ini}, C(t)_{atm}) = \sum_{t=1}^{T} [y(t) - E(t)x(t)]^T R(t)^{-1} [y(t) - E(t)x(t)] + C_{ini}^T P(0)^{-1} C_{ini} + \overline{C_{atm}}^T Q_m^{-1} \overline{C_{atm}} + \sum_{t=0}^{T-1} C(t)_{atm}'^T Q_a^{-1} C(t)_{atm}' \tag{1}$$

where C_{ini} and $C(t)_{atm}$ are the model initial state and atmospheric forcing, respectively, and are adjusted to reduce the cost function J. The first term on the right-hand side measures the uncertainty-weighted squares of model-data misfit, where $y(t)$ and $x(t)$ are vectors of observations and model state at time t, and $E(t)$ is the observation operator which maps the model state to the observations. The model $x(t)$ evolves with time by integrating the forward model with the first guess initial state, atmospheric forcing, and the corresponding increments C_{ini} and $C(t)_{atm}$. The last three terms are background terms for the initial state, time-averaged atmospheric forcing increments, and time-varying component of atmospheric forcing increments, giving confidence to the first guess initial state and atmospheric forcing. The overbars and primes in the last two terms in the right-hand side of equation (1) represent time-averaged and time-varying components. Superscript T is a matrix transpose operator. $R(t)^{-1}$, $P(0)^{-1}$, Q_m^{-1}, and Q_a^{-1} are the error covariance matrixes for the observations, initial state, time-

averaged atmospheric forcing increments, and time-varying atmospheric forcing increments. In this study, the error covariance matrixes are simplified to be diagonal filled individual variable error variance, and no covariance structures are assumed. Therefore, $R(t)^{-1}$, $P(0)^{-1}$, Q_m^{-1}, and $Q_a(t)^{-1}$ determines the relative contribution of each term to the total cost function. The definition of the errors will be introduced in section 3 and section 4.

To minimize the cost function (equation 1) with a large number of control variables ($\sim 8.2 \times 10^9$ within a 3-year assimilation window), we use an adjoint model to compute the gradients of the cost function with respect to the control vector. Here, we give a brief introduction to the adjoint model based Taylor Series and simple linear algebra.

Assuming that the cost function J is differentiable around C, effects of small control vector perturbations (ΔC) on the cost function J can be evaluated as equation (2) using Taylor expansion, where $\frac{\partial J}{\partial C}$ represents the first-order derivative, and $o(\Delta C)$ indicates the higher-order residual.

$$\Delta J = J(C + \Delta C) - J(C) = \frac{\partial J}{\partial C} \cdot \Delta C + o(\Delta C) \tag{2}$$

Note that ΔC is a vector with a dimension of $\sim 8.2 \times 10^9$. Assuming ΔJ equals one, with the first-order approximation, and taking the reverse of equation (2), we get,

$$\frac{\partial J}{\partial C}^* \cdot 1 = G(\Delta C) \tag{3}$$

The left-hand side term of equation (3) represents an adjoint model integration, which computes gradients descent directions and amplitudes $G(\Delta C)$. Then, a quasi-Newton algorithm based on Gilbert and Lemaréchal (2009) is adopted to efficiently reduce the cost function using the gradients $G(\Delta C)$. This process is being iterated until the cost function cannot be reduced or the cost function reduction differs by less than 1% in two consecutive iterations.

The adjoint code of MITgcm is generated by the Transformation of Algorithms in Fortran (Giering & Kaminski, 1998). Modifications are made on the adjoint code to ensure the usefulness of the adjoint model over a long assimilation window. Details of the modifications will be introduced in section 3.2.

2.3 Arctic Ocean Observing Systems

Despite recent improvements in the Arctic Ocean observing system over the past two decades, the Arctic Ocean remains one of the least explored regions of the world ocean due to the harsh environmental conditions and political difficulties. The Arctic Ocean observing network, which highly depends on satellite systems and in-situ observations, is limited by the existence of sea ice. In this study, we mostly evaluate the potential effect of the satellite observations, including sea surface temperature, ice concentration, ice thickness, and sea level anomaly products, and in-situ profiles from shipboard equipment and moorings on monitoring the Arctic Ocean changes. Table 1 lists information on parameters that are observed in the pan-Arctic Ocean. SST and along-track sea level anomaly (SLA) are available near-real-time and in the ice-free regions. Ice concentration is also near-real-time. These data are commonly used in operational ocean forecast. Hydrographic profiles are used by operational ocean forecast (e.g., Xie et al., 2017). However, it is very sparse and distributed unevenly in both spatial and temporal (Figure 1). Many more profiles are distributed in the Greenland, Iceland, and Norwegian (GIN) Seas than in the Arctic Ocean and more data available in the summer season than in the winter season. Mapped SLA over ice regions and mooring observations are

usually delayed by months to years and are not used in the data assimilation experiment. In this study, we perform data assimilation experiments based on all these observations.

Table 1. Parameters that observed by the Arctic Ocean observing systems

	Variables observed	Spacing	Sources
Datasets	SST	Gridded	AVHRR (Casey, 2010)
	Ice concentration	Gridded	ASI-AMSRE1 and ASI-SSMI2(Spreen et al., 2008)
	Ice thickness	Gridded	CryoSat-SMOS merged data (Ricker et al., 2017)
	Hydrographic profiles 1	Point	EN4 (Good et al., 2013) and UDASH (Behrendt et al., 2018)
	SLA	Track	C3S
	Monthly SLA	Gridded	Mapped-data from DTU (Rose et al., 2019)
	Moorings2	Point	Bering Strait (Woodgate et al., 2012), The Fram Strait (Schauer et al., 2008), BGEP (Proshutinsky et al., 2009), NABOS (Baumann et al., 2018; Dmitrenko et al., 2008)

3. Observing System Simulation Experiments (OSSEs)

Observing System Simulation Experiments (OSSEs) are important tools to test the potential effects of new or existing observations on operational weather and ocean forecast before the instruments are built or deployed (Errico et al., 2013). In a well-observed system, one can perform such an experiment based on true observations. Given that the Arctic is undersampled, we have to rely on synthetic observations generated through a model simulation which also called "nature run". Using such a nature run as the true state, we create pseudo-observations based on existing observing systems and a purposed observing system with realistic uncertainties. Then, data assimilation experiments with and without the new observations are performed. The potential effects of the new observations on the reanalysis and forecast are evaluated by comparing the assimilation results with the nature run.

In this section, we perform two OSSEs to evaluate the effects of the near-real-time Arctic Ocean observing system on the ocean synthesis and additional effects from moorings and mapped SLA over the ice cover region. A 4-km Atlantic-Arctic ocean simulation (section 2.1) is used as the nature run to generate pseudo-observations. Pseudo-observations (Table 2) are simulated based on the real observing systems (Table 1) and the nature run. Table 2 lists observations that are assimilated in the two assimilation experiments. Expt01 assimilates near-real-time observations that are widely used in operational ocean forecast. Delayed observations from moorings and mapped SLA over sea ice cover regions (Armitage et al., 2016; Rose et al., 2019) may also provide valuable information. We evaluate their potential effects on the ocean synthesis in expt02.

Table 2. Observations assimilated in the two OSSEs

	Expt01	*Expt02*	*Instrument errors*
Datesets	Sea surface temperature	Sea surface temperature	0.35 °C
	Ice concentration	Ice concentration	10%
	Ice thickness	Ice thickness	0.2 m
	Hydrographic profiles	Hydrographic profiles	Temperature 0.02
			Salinity 0.02
	Daily sea level anomaly	Daily sea level anomaly	3 cm
		Monthly sea level anomaly	3 cm
		Moorings[1]	Temperature 0.02
			Salinity 0.02

[1] Locations of moorings are marked by red dots in Figure 1; we assume that the moorings observe temperature and salinity profiles from 50m-1000m.

3.1 Simulation of Observations and Uncertainties

The pseudo-observations and their uncertainties are important to evaluate their potential effects in the OSSEs. Based on the daily output of the nature run and spatiotemporal distribution of observations (Table 1 and Table 2), we generate pseudo-observations. We assume the observation errors consist of instrument errors and representative errors. Instrument errors take a Gaussian distribution with the variances listed in Table 2, and the errors are added to individual observation types when generating the pseudo-observations. Representative errors denote errors due to unresolved processes in the model. In this study, they are computed using the nature run with the method described in Oke and Sakov (2008). For SST, ice concentration, ice thickness, and SLA, spatial distributions of representative errors are used. Shown in Figure 2 is the representative errors for SST and ice concentration. The figure reveals that representative errors are much larger than the instrument error along the ice edge regions. Along the East Greenland Current, SST error and ice concentration error can be as large as 2.5 °C and 0.2, respectively. For temperature and salinity profiles from EN4 and moorings, a vertical error profile is used, which is ~0.57 °C and ~0.28 PSU at the surface and reduces to ~0.02 °C and 0.02 PSU in the bottom layer.
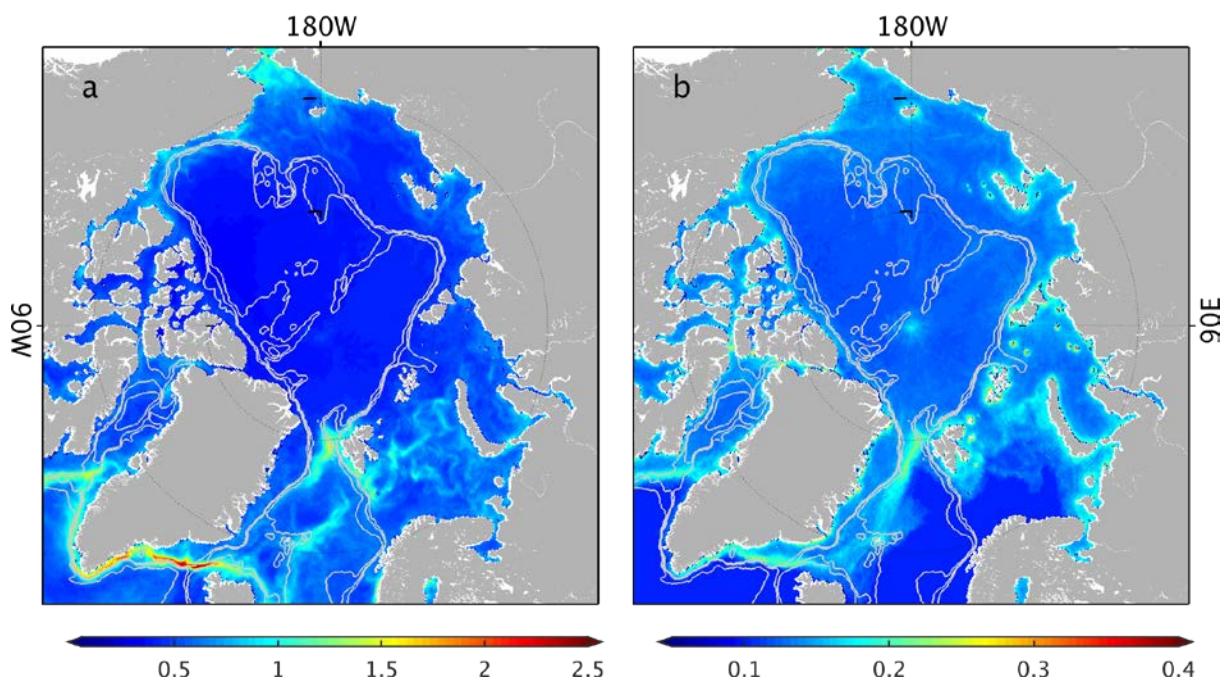

Figure 2. Spatial distributions of representative error for SST (a) and ice concentration (b).

In this study, we take daily increments for 2 m air temperature, 2 m specific humidity, precipitation rate, 10 m wind vectors, downward longwave radiation, and net shortwave radiation as control variables and adjust them to reduce the cost function J. In the OSSEs and the first chunk of the 10-year synthesis, initial temperature and salinity are also adjusted to reduce the cost function. A 3-year (2004-2006) assimilation window is used. This configuration leads to 8.2×10^9 elements in the control vector. Uncertainties for increments of the time-varying atmospheric forcing (Q_a) are computed as the standard deviation of the NCEP RE1 data. And for the time-average components (Q_m) of 2 m air temperature, 2 m specific humidity, precipitation rate, 10 m wind vectors, downward longwave radiation, and net shortwave radiation, their uncertainties are set to 1 °C, 0.001 kg/kg, 1.5×10^{-8} m/s, 2 m/s, 20 W/m^2, 20 W/m^2.

3.2 Validation of the Tangent Linear Approximation

To ensure the numerical stability of the adjoint model, previous studies (Mahfouf, 1999; Zhu et al., 2002) have found that some physical terms, such as parameterized vertical mixing coefficients, radiation processes, internal sea ice stress tensors, must be disabled in the adjoint code. Therefore the following modifications are made in the adjoint model:

1) excludes the K-profile mixing parameterization scheme;
2) simplify the sea ice dynamics submodel to a free drift model, and
3) increase the Laplacian diffusivity of heat and salinity to 500 m^2/s, and lateral eddy viscosity to 10000 m^2/s.

The first two modifications have been extensively examined when applying the 4D-var data assimilation method to short-term ocean prediction. Linearizing these highly nonlinear terms lead to instability of the adjoint model, rendering the adjoint sensitivity useless for the optimization. With these simplifications, the adjoint model can usually provide useful gradients for the minimization algorithm within the predictability limit of the nonlinear system.

The third modification intends to extend the assimilation window beyond the predictability of the nonlinear system. We increase diffusivity and viscosity coefficients to suppress the exponentially growing of adjoint sensitivities related to fast-growing modes (.e.g., eddies in an eddy-resolving model) of the nonlinear system (see details in Hoteit et al., 2005; Köhl & Willebrand, 2002; Sugiura et al., 2015).

Both the tangent linear approximation and the above modifications introduce errors in the gradients of the cost function J with respect to the control variables, which are vital for minimizing the cost function. Therefore, it is necessary to test the usefulness of this approximate tangent linear approximation (section 2.2) with our model configuration because of the strong nonlinearity of sea ice processes. A practical way is comparing the spatial-temporal error evolution based on several forward model runs, and the modified tangent linear model runs with prescribed perturbations on the control variables.

We use the atmospheric forcing increments from the synthesis work of Koldunov et al. (2017) as errors to perturb the forward model and the approximate tangent linear model. We perform three forward runs from the year 2004, in which atmospheric forcing variables are perturbed. The first forward run F($C(t)_{atm}$) is forced with atmospheric forcing. The second and third forward runs are performed by adding ($F(C(t)_{atm} + \Delta C(t)_{atm})$) and subtracting $F(C(t)_{atm} - \Delta C(t)_{atm})$ the realistic perturbations from the referencing atmospheric forcing. Then, the differences between the perturbed model runs and the reference model run are computed as follows,

$$\Delta F_1 = F(C(t)_{atm} + \Delta C(t)_{atm}) - F(C(t)_{atm}) = \frac{\partial F}{\partial C} \cdot \Delta C(t)_{atm} + o(\Delta C(t)_{atm}) \qquad (4)$$

$$\Delta F_2 = F(C(t)_{atm} - \Delta C(t)_{atm}) - F(C(t)_{atm}) = -\frac{\partial F}{\partial C} \cdot \Delta C(t)_{atm} + o(-\Delta C(t)_{atm}) \qquad (5)$$

Based on equations (4) and (5), the first and second derivatives of the nonlinear error propagation can be obtained by $\frac{1}{2}(\Delta F_1 - \Delta F_2)$ and $\frac{1}{2}(\Delta F_1 + \Delta F_2)$. By integrating the tangent linear model with the above atmospheric forcing perturbations, we can directly get error evolution for all model variables.
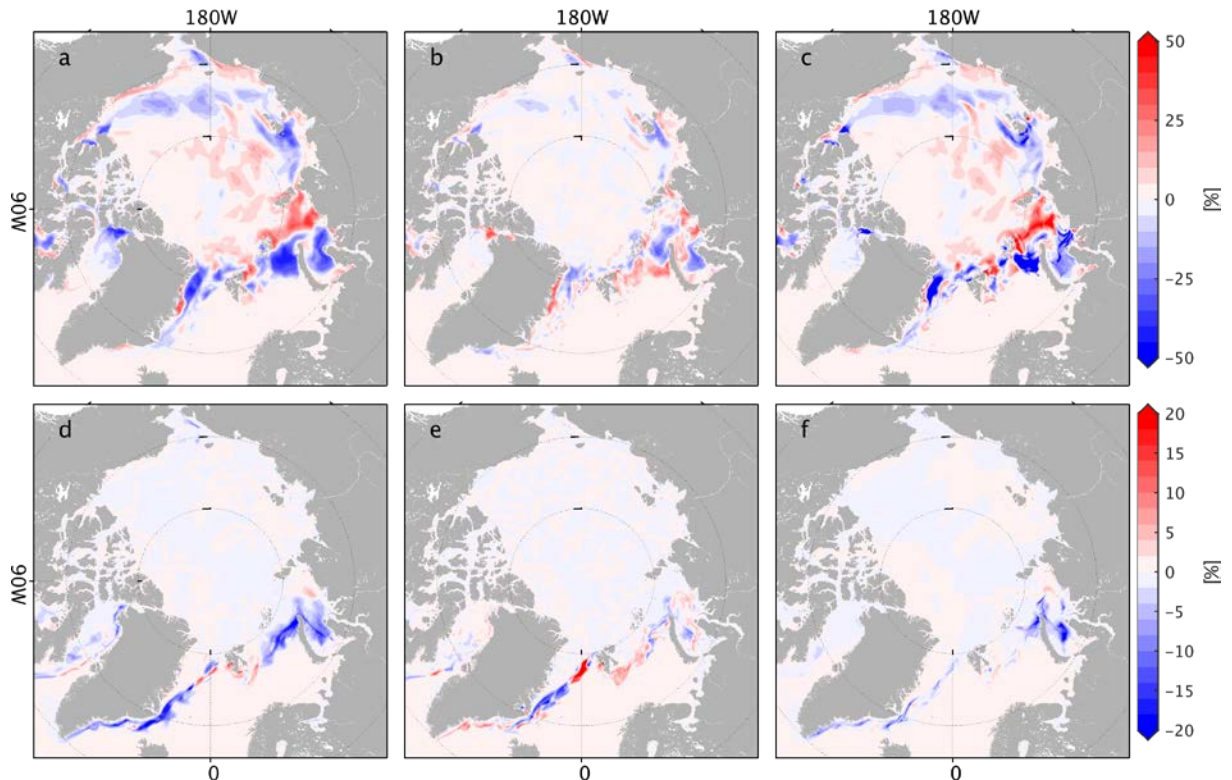
Figure 3. Linear (a) and nonlinear (b) components sea ice concentration errors averaged over May and June computed based on equations (4)-(5). Panel (c) is the sea ice concentration error predicted by the approximate tangent linear model in May and June. Panels (d)-(e) are the same as panels (a)-(c), except that they are sea ice concentration error averaged over November and December.

Figure 3a-c show the linear component $\frac{1}{2}(\Delta F_1 - \Delta F_2)$ (a), the higher-order component $\frac{1}{2}(\Delta F_1 + \Delta F_2)$ (b), and the tangent linear model predicted sea ice concentration changes in the summer season. Sea ice changes due to the atmospheric forcing perturbations are significant in both the marginal seas and the deep ocean. The linear component (a) accounts for more than 80% of the sea ice concentration changes, and the tangent linear model predicts more than 90% of the linear component of the changes. In the wintertime (Figure 2d-f), significant sea ice changes exist along the ice edge, including the East/West Greenland Current, in the Barents Sea, and the Kara Sea. Both the linear component (Figure 2d) and the higher-order component (Figure 2e) are important, with the linear component account for more than 60% of the total changes. In this case, the tangent linear model (Figure 2f) can only predict ~40% of the linear error. In both the two cases, the higher-order sea ice concentration changes exist in the ice edge, indicating that the nonlinear dynamics are prominent over these regions. The results above show that the linear component dominates the sea ice changes, and the nonlinear part mainly takes effects in the ice edge regions. The tangent linear model could capture the linear mode of the sea ice changes reasonably well considering the directions. However, the tangent linear model underestimates the amplitude of the sea ice changes up to 50% in the winter season, which may degrade the usefulness of the adjoint model.

3.3 Results

In this section, we analyze the impacts of assimilating pseudo-observations, sampled based on existing Arctic Ocean observing system and ATLARC04km simulations, on the model simulations. We assess the performance of optimization in section 3.3.1. Changes of the control variables, sea ice parameters, ocean temperature, and salinity will be shown below.

3.3.1 Evaluation of the optimization

In both expt01 and expt02, 18 iterations are performed, respectively. Figure 4 shows the resulting reduction of the total cost function and individual constitutes (black bars) and the residual root mean square (RMSE) errors (grey bars) in the two experiments. Overall, the cost function is reduced by ~37% (expt01) and ~40% (expt02). In terms of individual constitutes, sea ice concentration (SIA), sea surface temperature due to sea ice (SIA-SST), and sea ice thickness (SIT) contribute most to reduce the total cost function. SLA error is also considerably reduced. In expt02, errors of mooring-observed temperature (Moor-T) and salinity (Moor-S) are also significantly reduced. The other constitutes are only slightly reduced. After the assimilation, errors of variables that are assimilated in both expt01 and expt02 are reduced to a similar level. The reduction of errors in the mooring observations is significant in expt02.
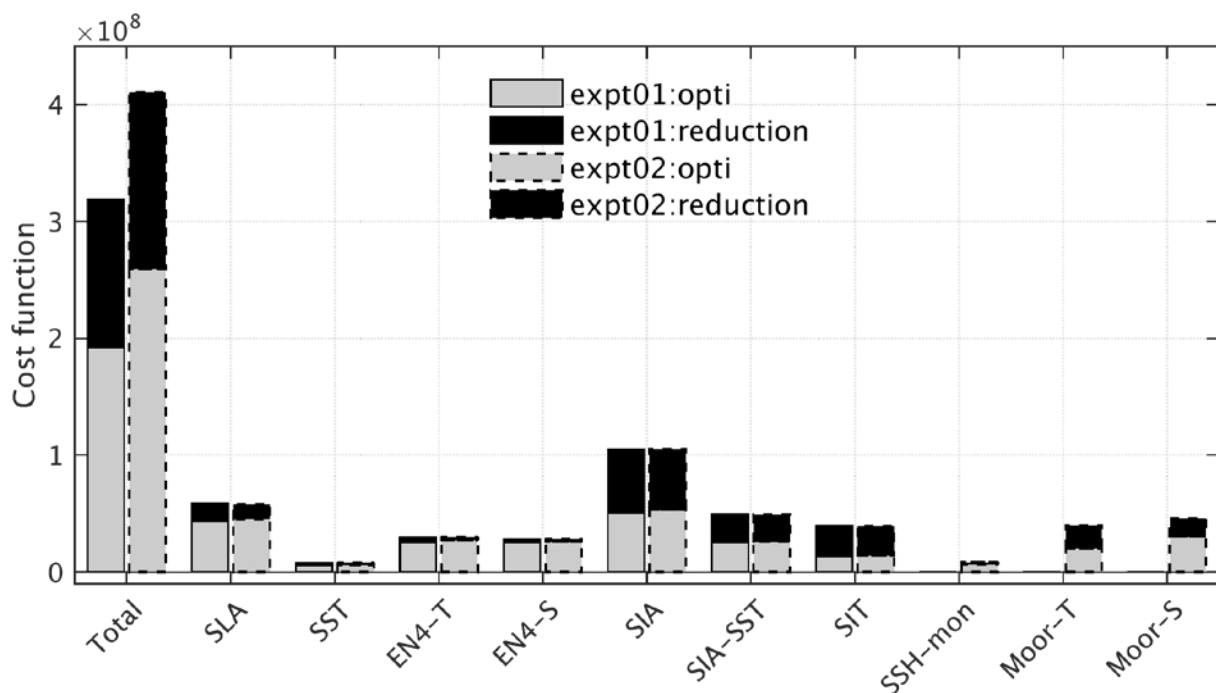

Figure 4. Reduction (black bars) of the total cost function and individual variables, and the cost function and individual component after the last iteration (grey bars). Bars with solid and dashed edges are for expt01 and expt02, respectively.

3.3.2 Sea ice improvements

Shown in Figure 5 are time series of total sea ice concentration and volume over the pan-Arctic Ocean in the nature run, control run, and the two assimilation experiments. The control run simulates more sea ice than the nature run over the whole period. Figure 5a reveals that both the two assimilation experiments successfully bring the sea ice concentration into consistency with the nature run. In the summer season, sea ice concentration is significantly reduced while its changes are tiny in the winter season. Total sea ice volume, as shown in Figure 5b, is also improved in both the two assimilation experiments, and the

improvement is significantly over the entire period. Although sea ice thickness observations are assimilated in the winter season, we note that sea ice volume in the assimilation experiments matches better with the nature run in the summer season than the winter season.
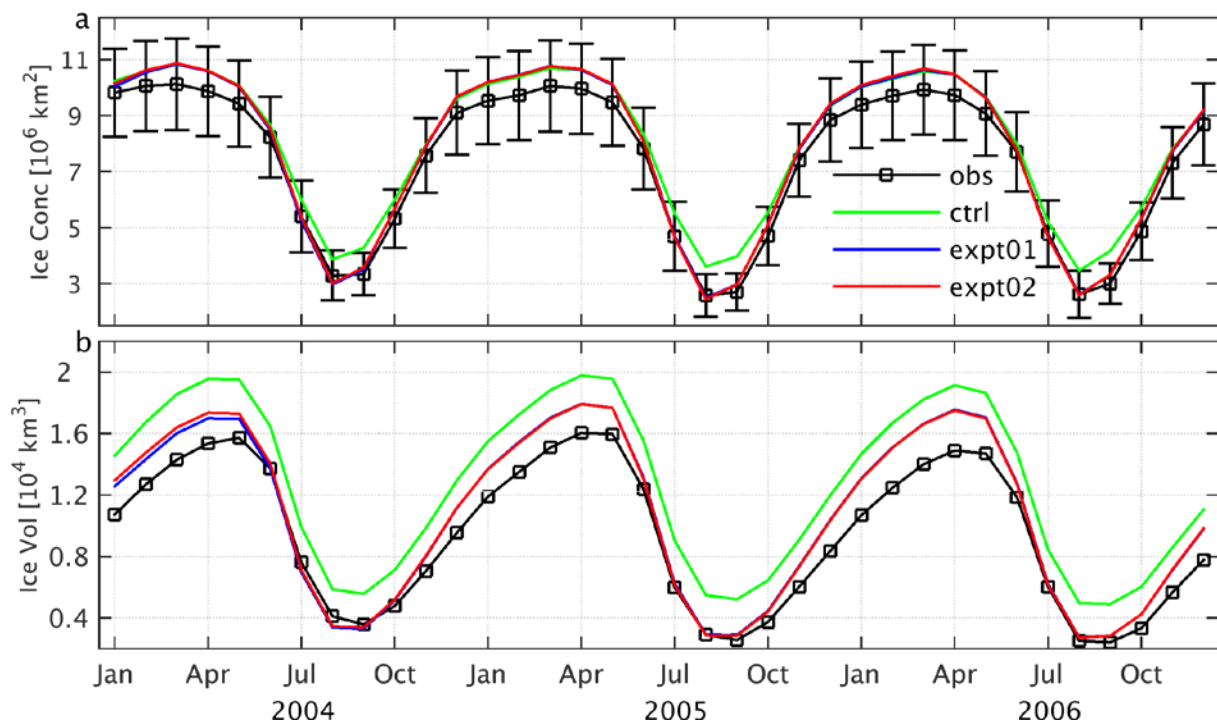
Figure 5. Time series of (a) total sea ice concentration and (b) total ice volume over the pan-Arctic Ocean in the nature run (obs), control run, expt01, and expt02.

To better illustrate the spatial distribution of sea ice concentration and thickness improvements, we show in Figure 6, sea ice concentration and thickness errors in the control run and the two assimilation experiments. In the summer season, the control run (Figure 6a) overestimates sea ice cover up to 30% in a large area of the Arctic Ocean and underestimates sea ice cover ~10% around Franz Josef Land. Both expt01 (Figure 6b) and expt02 (Figure 6c) significantly reduce the errors except along the northeastern and northern Greenland coast. In the winter season, negative sea ice concentration error (-30%) in the control run exists in the sea ice edge regions, including the Barents Sea and along the East Greenland Current. The two assimilation experiments (Figure 6e and f) slightly reduce the errors by ~15%. But significant sea ice errors remain in these regions. The reason for the remaining errors may be related to the reduced performance of the adjoint model in the winter season (Figure 3d-f) along the sea ice edge. Sea ice thickness error (Figure 6g) is also remarkably reduced in expt01 (Figure 6h) and expt02 (Figure 6i), especially in the deep-sea region. Remaining sea ice thickness errors mainly located in the shallow water regions, including the Kara Sea, the Laptev Sea, the East Siberian Sea, and along the East Greenland Sea Current.
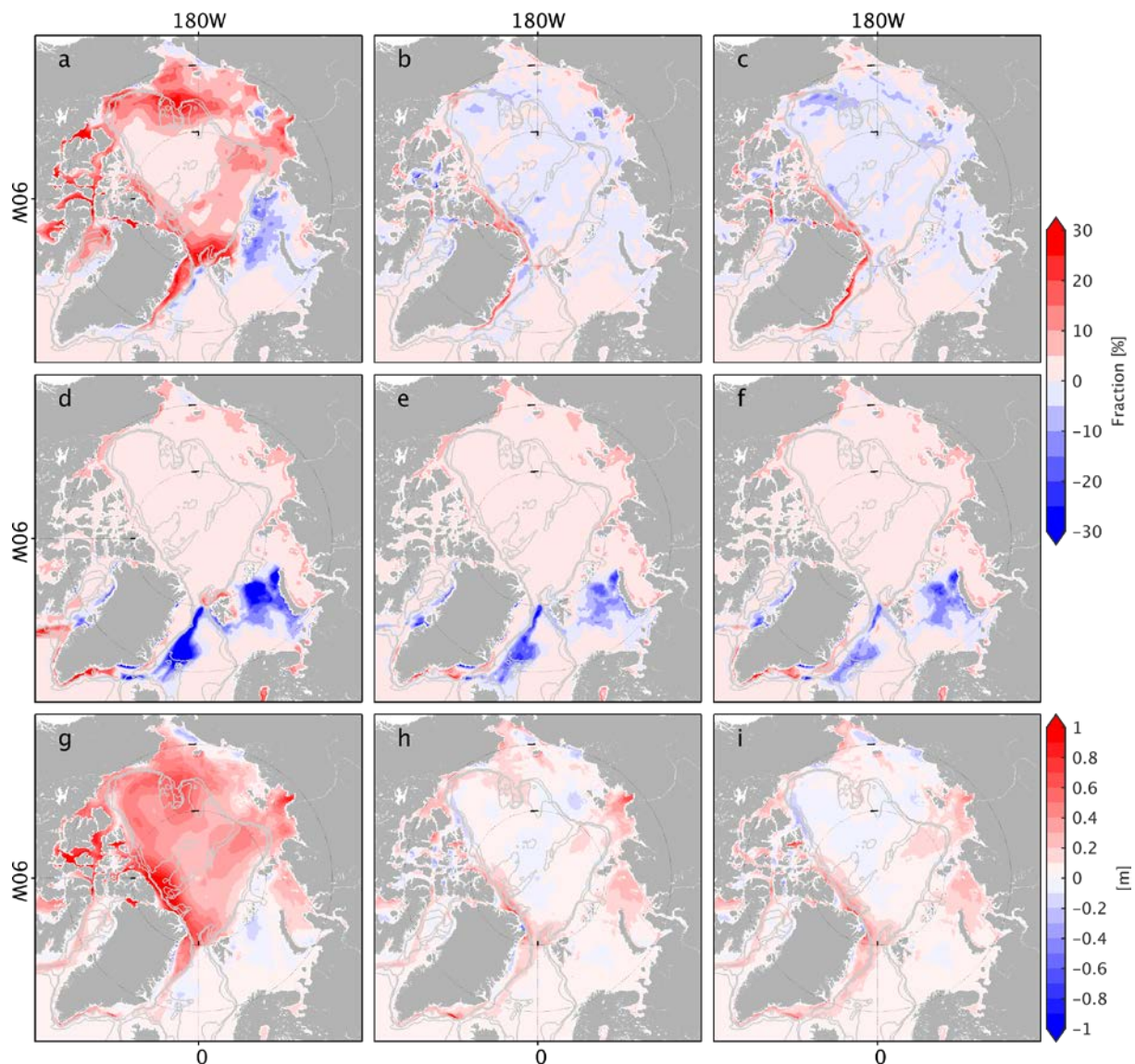
Figure 6. Sea ice concentration difference between the control run and the nature run (a), between expt01 and the nature run (b), and between expt02 and the nature run (c) in the summer season. (d)-(f) are the same as (a)-(b) but in the winter season. (g)-(i) are for sea ice thickness error over the entire assimilation period.

3.3.3 Temperature and Salinity Changes

Temperature and salinity observations in the Arctic Ocean rely on shipboard equipment and are much less than the rest of the world Ocean. Changes in sea ice can also change the temperature and salinity of the Ocean by modifying the air-sea interaction and releasing freshwater to the ocean (G. et al., 1998; Giles et al., 2012; Polyakov et al., 2010). Changes in temperature and salinity are much smaller than the sea ice components. In this section, we assess the improvement of assimilating pseudo-observations from existing observing systems on salinity and temperature.

In the top layer (<50m), the temperature in the control run (Figure 7a) is warmer than the nature run in the Arctic Ocean and the GIN seas but is colder in the Labrador Sea. Temperature increments in expt01 (Figure 7b) reveal that temperature errors in the GIN seas, the Barents Sea, the Labrador Sea, and near the Bering Strait are reduced. However, the positive temperature error in the Arctic Basin is slightly increased. In expt02 (Figure 7c), further reduction of temperature error in the GIN seas, especially along the Norwegian Atlantic Current and the East Greenland Current, is significant. The improvement is likely related to assimilating the moorings deployed in the Fram Strait. Over the ice-cover regions,

the temperature is slightly degraded, which is probably caused by enhanced air-sea interaction related to the reduction of the sea ice cap.

In the middle layer (50-500m), the temperature error pattern (Figure 7d) is similar to that in the upper layer (Figure 7a) except that temperature in the control run shows a negative bias on the pathway of the Atlantic inflow north of Franz Josef Island. In expt01, reductions of temperature errors in the GIN seas, the Barents Sea, and the Labrador Sea are still visible. Slight improvement along the East Siberian Sea continental slope is also noticeable. However, north of Svalbard, positive temperature error is increased in expt01. Figure 7f shows the temperature difference between expt01 and expt02. Further improvements are located along the Norwegian Atlantic Current, the East Greenland Current, the pathway of the Atlantic inflow through the Fram Strait, which is likely caused by assimilating the Fram Strait mooring observations. In the Makarov Basin and the Beaufort Sea, small temperature error reductions are also visible.
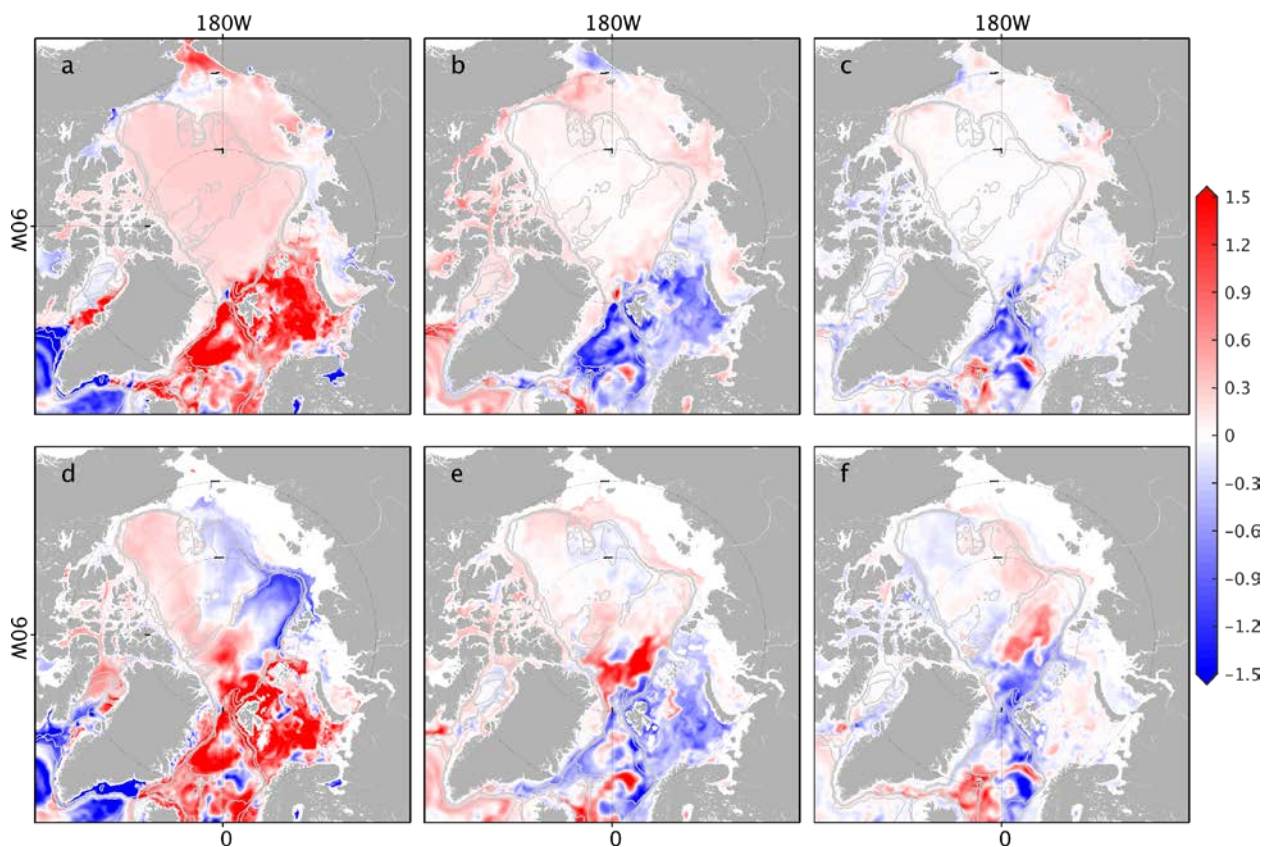
Figure 7. The seawater temperature difference between the control run and the nature average over the upper 50m (a) and 50-500m (d). Panels (b) and (e) are the temperature increments in exp01. (c)-(f) are the temperature difference between expt02 and expt01.

The reduction of seawater salinity is limited in the upper layer (Figure 8). Seawater in the top layer is much saltier in the control run than that in the nature run over the entire Arctic Ocean (Figure 8a). Salinity error reduction in expt01 (Figure 8b) is located in the Greenland and Iceland Seas, large areas of the Arctic Ocean. The reduction of salinity is likely related to the decrease of sea ice, which releases freshwater into the ocean and is transported via circulation. Figure 8c reveals that expt02 further reduces salinity errors near mooring locations in the Beaufort Sea and along the pathway of Atlantic inflow while degradations are found in central Nansen Basin, north Canadian Basin, and East Siberian Basin. The improvements are likely to result from the addition of mooring observations. To reduce the

mooring cost component, freshwater from the sea ice melting is transport to the mooring locations by adjusting control variables.
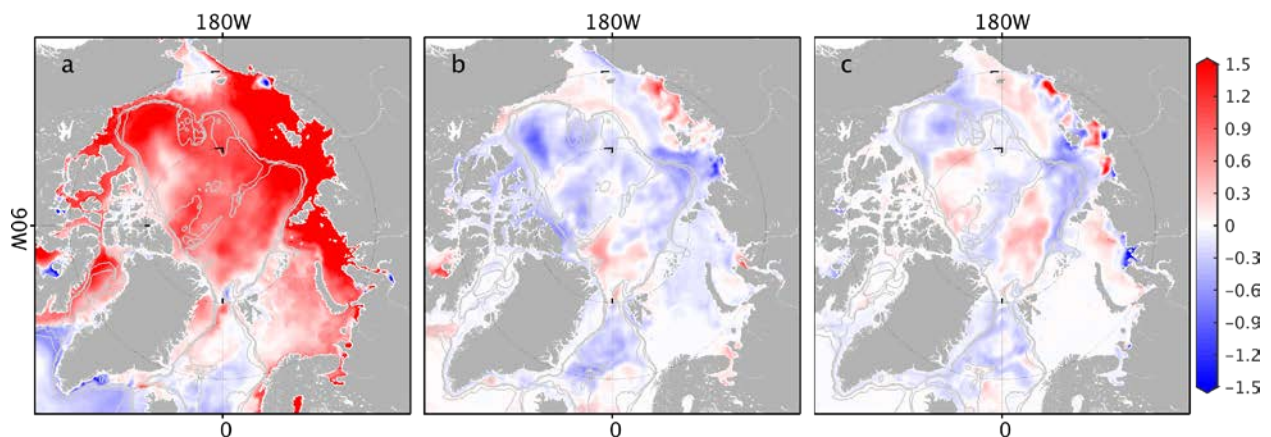
Figure 8. Seawater salinity difference between the control run and the nature average over the upper 50m (a). (b) and (c) are the salinity difference between expt01 and the control run and between expt02 and expt01.

3.3.4 Control Variables

As introduced in section 2.2, control variables are adjusted to bring the model simulation close to available observations. Increments of the control variables contain important information on how they are adjusted to reduce the model-data difference, revealing the relative importance of different atmospheric forcing on changing ocean-sea ice state. Based on the results of expt02, we add increments of wind vectors, 2 m air temperature, and initial temperature and salinity one by one to the atmospheric forcing and evaluate the contribution of the individual component on the cost function reduction. Subsequently, we analyze the increments of the control variables in expt01 and expt02, explaining how they are adjusted to change the ocean-sea ice state.

Listed in Table 3 is the reduction of the cost function and each constitutes, and contributions from increments of wind vectors, 2 m air temperature, initial temperature and salinity, and the other control variables. The optimization reduces all the components of the cost function except for monthly SLA fields. However, it only accounts for ~1.5% of the total cost function.

Of all the control variables, adjustment of wind, and initial condition dominate the total cost reduction. 2 m air temperature also considerably reduce the cost function, especially sea ice thickness errors. The other control variables, including 2 m specific humidity, precipitation rate, downward longwave radiation, and net shortwave radiation only contribute ~3.9% of the total cost function reduction and are not sensitive to cost functions.

Increments of wind vectors dominate the reduction of individual cost function components, except for sea ice thickness, sea ice SST, and mooring observations. Sea ice thickness improvement is governed by both 2 m air temperature (34.6%) and the initial conditions (32.8%). Improvements in SIC(SST) and mooring observations are attributed to wind and the initial condition increments, with the initial state dominating. Sea ice concentration, which contributes most to the total cost, is improved by adjustment of wind (53.8%), 2 m air temperature (22.6%s), and initial temperature and salinity(21.9%).

Table 3. Reduction of the total cost function and each component (second column) and contributions from increments of wind (third column), 2m air temperature (fourth column), initial salinity and temperature (fifth column), and the other control variables (the last column) in expt02.

	Cost function reduction (%)	Contribution of the control variables to the cost function reduction (%)			
		wind	2m Air temperature	Initial condition	Others
Total	36.7	45.0	13.0	38.2	3.9
SLA	22.5	75.4	-4.5	24.3	4.8
SST	29.5	54.2	18.0	24.1	3.8
EN4(T)	9.9	59.3	11.3	25.8	3.6
EN4(S)	7.6	46.0	4.0	45.7	4.4
ICE(Con)	49.1	53.8	22.6	21.9	1.7
ICE(SST)	47.1	50.4	-3.3	56.5	-3.6
ICE(THK)	64.4	18.3	34.6	32.8	14.3
SSHm	-37.4	-18.6	-8.8	1.3	-1
Mooring(T)	50.1	28.8	-4.0	72.8	2.5
Mooring(S)	34.1	42.2	2.2	50.9	4.8

Shown in Figure 9 are the initial temperature increment in expt01 and expt02-expt01 in the top 50m (a,b) and 50-500m (c,d). In the top 50 m, a significant positive temperature increment occurs over the ice-cover regions (Figure 9a) despite the positive temperature bias (Figure 7a) in the pan-Arctic Ocean. Comparing the patterns of initial temperature adjustment with sea ice concentration and thickness errors in Figure 6, we see that the change in the initial temperature contributes to reducing the sea ice concentration and thickness errors. Initial temperature adjustment below 50 m (Figure 7b) is small and is located along the continental slope of the East Siberian Sea, the Barents Sea, and ice edge regions. Comparing further adjustment of initial temperature (Figure 9b and d) with temperature changes (Figure 7c and f), we identify that temperature along the pathway of the Barents Sea branch of Atlantic inflow is increased, which reduces the negative bias of Atlantic inflow north of Franz Josef land. This long-lasting signal is likely captured by moorings deployed in the continental slope of the Laptev Sea because warm water that enters into the Barents Sea submerges beneath the cold water and isolated to the atmosphere.

Significant signals also exist in other regions of the Arctic Ocean. However, these additional signal is likely damped out quickly and are invisible in the temperature changes in Figure 7c and f. Overall, adjustment of initial temperature increment is mainly over the ice-cover region and contribute to ice parameter changes. With additional mooring observations in expt02, temperature along the Barents Sea branch of the Atlantic inflow is increased to reduce the negative bias of the Arctic Atlantic Current north of Franz Josef Land.
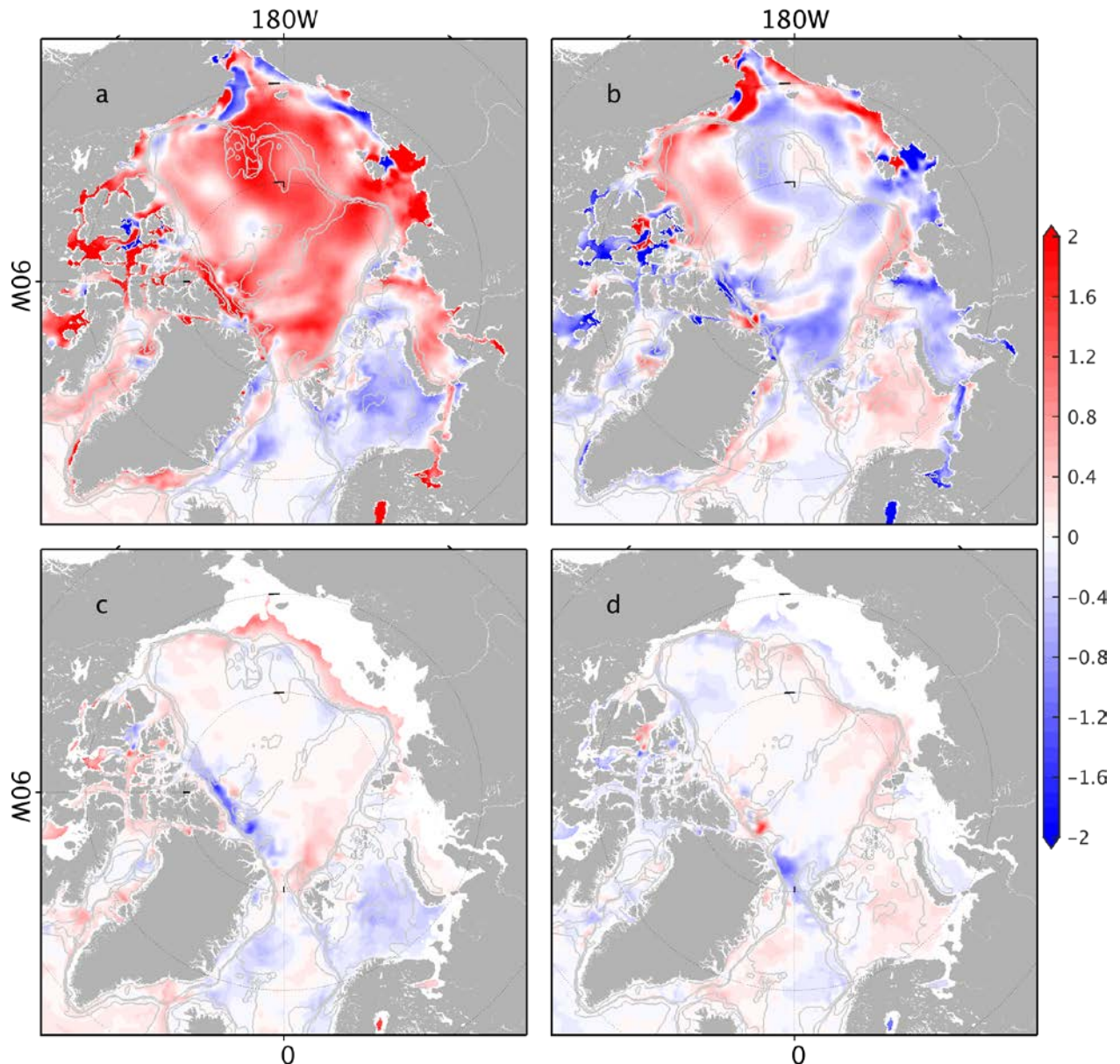
Figure 9. Adjustment of initial temperature over the upper 50m and 50-500m in expt01 (a,b), and the difference between expt02 and expt01 (c,d).

Similar to the initial temperature adjustments, 2 m air temperature (Figure 10a) also shows positive change over the ice cover region and negative adjustment in the Barents Sea. It is adjusted to reduce sea ice concentration and thickness errors (Table 3). Additional adjustment of 2 m air temperature in expt02 (Figure 10b) is small and locates in the coastal regions and near the location of moorings.

Unlike all the other control variables, corrections to the zonal and meridional wind (Figure10c and e) exist in the region with significant ice concentration errors. Additional adjustment of wind vectors in expt02 is also substantial (Figure10d and f) in the marginal seas, in the Beaufort Sea, and along the pathway of the circulation. Corrections of wind vectors intend to reduce sea ice concentration and, at the same time, redistributing the freshwater to the mooring locations.
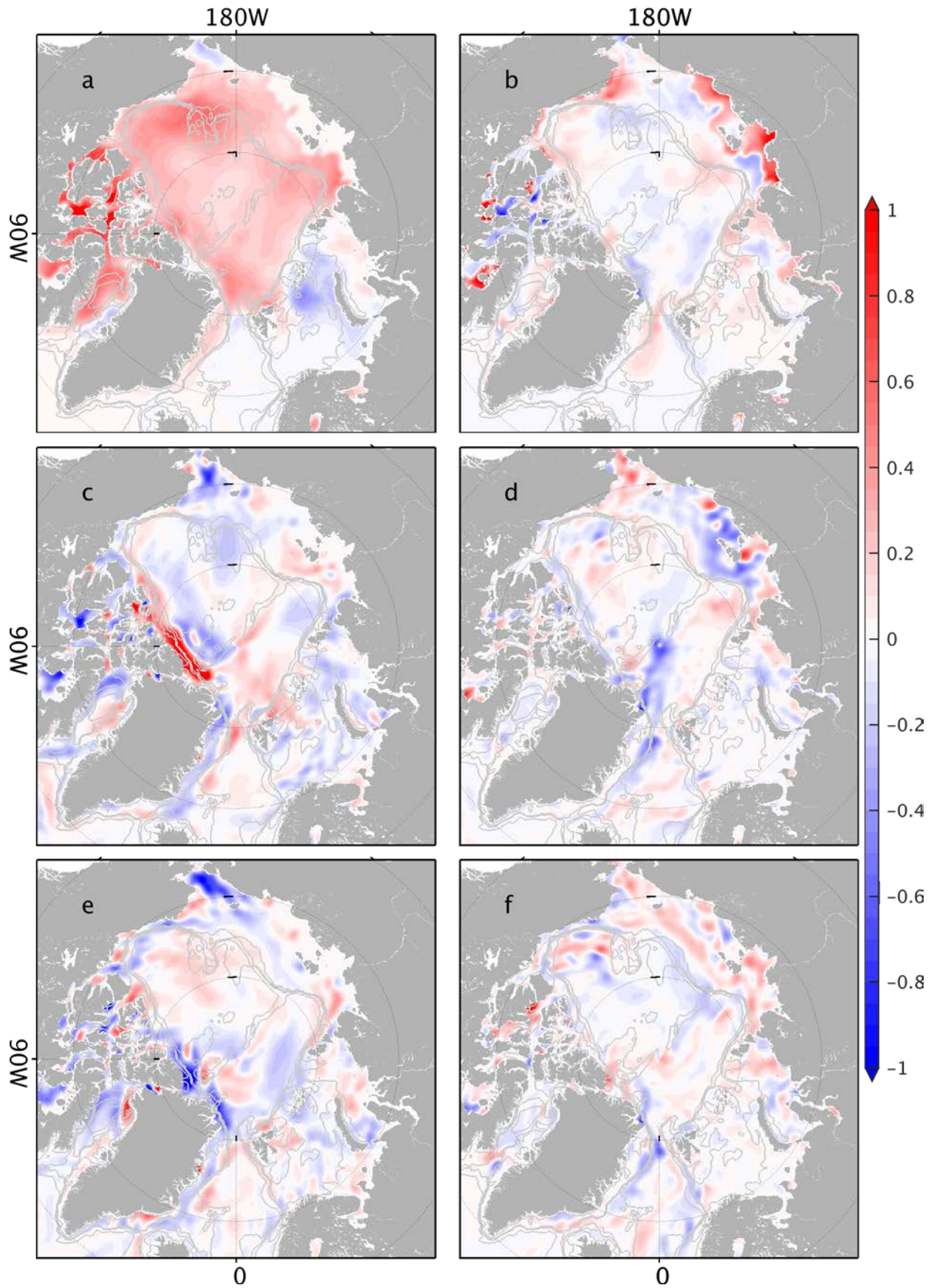
Figure 10. Time-averaged 2 m air temperature increment in expt01 (a), and the difference between expt01 and expt02. (c)-(d) and (e)-(f) are the same as (a)-(b) but for u wind and v wind components.

3.3.5 Increasing Profile Observations

In this study, hydrographic profiles are sampled based on data over the year 2003-2006. Since the year 2007, hydrographic profiles are almost doubled (Behrendt et al., 2018) with international efforts. To evaluate the potential effect of increasing the number of profiles, we resampled the profiles in expt02 with available profiles in the year 2008. Starting from the last iteration of expt02, we run the adjoint model based on the new profiles data.

Shown in Figure 11 is the adjoint sensitivity for initial temperature and u wind in expt2 (b,d), and expt2 with new profile data (a,c), which play a significant role in reducing the profile constitute of the cost function (Table 3). The figure reveals that an increasing number of profiles have little effect on the gradient patterns of initial temperature and u wind. Therefore, the data assimilation cannot extract more information from the profile observations. The gradient patterns still represent ice concentration error patterns, and the optimization will again try to reduce sea ice concentration error in the following iterations. Therefore, even in-situ profiles are increased during the period of "The Fourth International Polar Year" with international efforts, temperature and salinity observations are still too few to well constrain the solution.
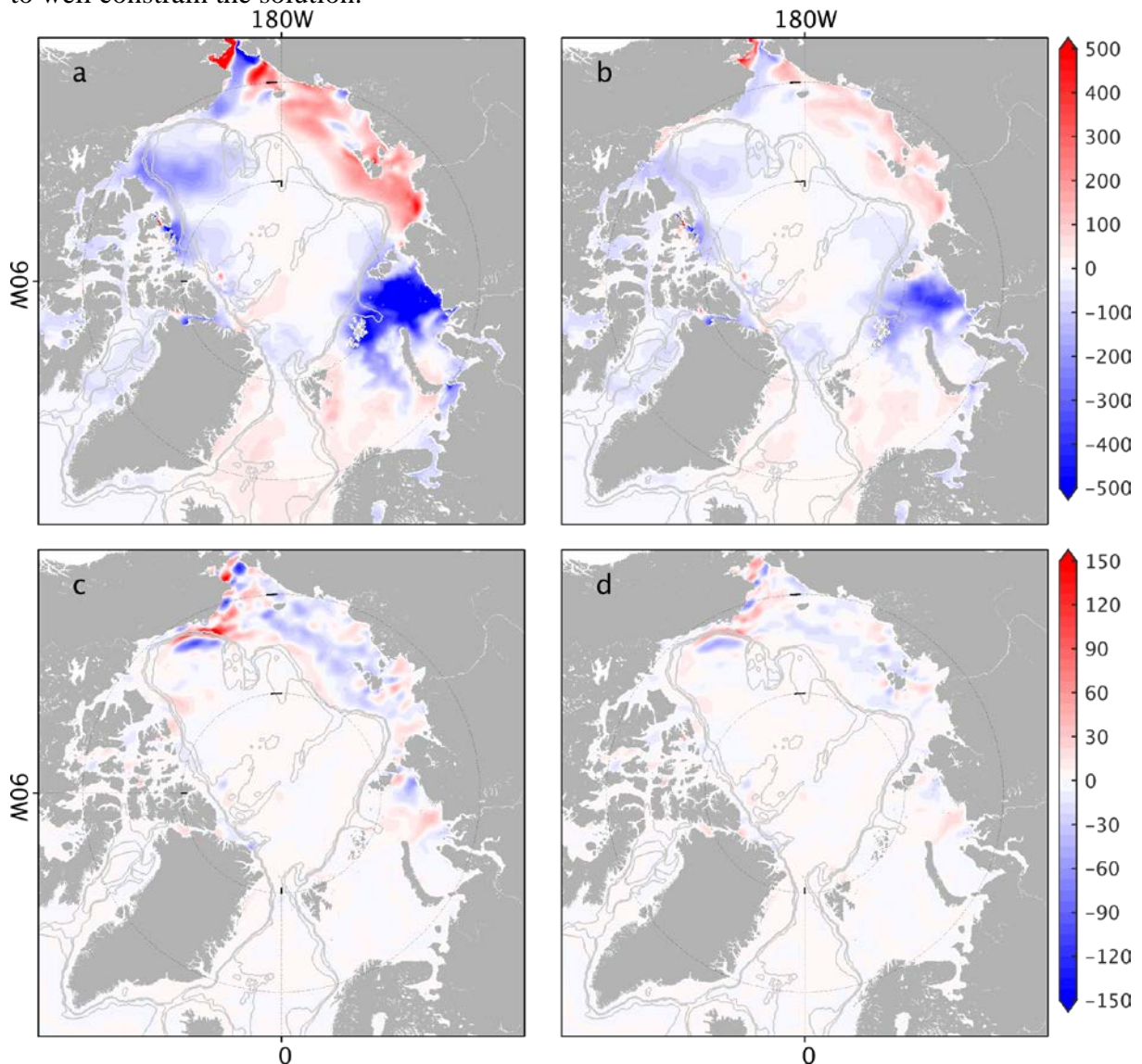
Figure 11. Gradients of the cost function with respect to initial temperature (a, b) and u wind averaged the assimilation period (c,d). The difference between the left column and the right column is the profiles used in the cost function. In the left column, profile observations are sampled based on the 2008 profiles data. And profiles are sampled using the year 2004-2006 data. The two runs are based on the last iteration of expt02.

3.4   Concluding remarks

We perform two OSSEs to assess impacts of assimilating near-real-time pan-Arctic Ocean observations and together with delayed data from moorings and monthly mapped SLA data on monitoring the Arctic Ocean changes. Pseudo-observations and their uncertainties are generated according to a 4-km Atlantic-Arctic simulation and the spatiotemporal coverage of various observing systems. The observations are then assimilated into a 16-km pan-Arctic ocean model using the adjoint method and a 3-year assimilation window. The improved simulation is validated against the 4-km Atlantic-Arctic simulation.

Results show that both ice concentration and ice thickness are significantly improved after data assimilation. Most of the sea ice concentration improvement occurs in the summer season over the entire Arctic Ocean. In the winter season, sea ice concentration error mainly exists near the ice edge regions, and the data assimilation slightly reduces the error, which may be related to the weak performance of the adjoint model in these regions. Sea ice thickness is significantly improved in the central Arctic Ocean. However, errors remain in the marginal seas and around Greenland. Ice volume after data assimilation matches the nature run well, especially in the summer season.

Improvements in the seawater temperature occur in ice-free and near ice edge regions. Additional effects of moorings deployed in the Fram Strait and at the continental slope of the Laptev Sea are visible. Salinity changes mainly occur in the upper layers over the ice-cover regions, which are likely as a result of ice volume reduction. Further improvements near the mooring locations are also visible but it is accompanied by degradation in the other areas.

The adjustment of wind vectors dominates the total improvement, and most of the individual constitutes. Corrections of initial condition dominate error reduction of mooring observations, especially in the continental slope of the Laptev Sea and the Fram Strait, reflecting the long memory of the Atlantic inflow. Moorings deployed in the inflow paths provide information about the circulation upstream of preceding years.

The improvements in sea ice concentration and thickness indicate that sea ice processes seem to be the dominant mode in the Arctic Ocean. By assimilating pseudo-observations from existing observing systems, their errors are significantly reduced, especially in the summer season. Remaining errors along ice edge regions may relate to the weak performance of the adjoint model.

4.   A 10-year Arctic Ocean-Sea ice Synthesis

Koldunov et al. (2017) produced a synthesis by assimilating near-real-time observations from the year 2000 to 2008 with an assimilation window of 1 year. Over the past decade, more observations are available, such as moorings, monthly mapped SLA (Armitage et al., 2016; Rose et al., 2019). In this study, we will extend the synthesis from the year 2007 to 2016 and assimilate all available observations.

Assimilated observations are shown in Figure 12. A 4-year assimilation window is used, and the whole synthesis period is divided into three chunks: 2007-2010, 2010-2013, 2013-2016. The control vectors include daily atmospheric forcing on the model grid, which is linearly interpolated to model time and which includes 2 m air temperature, 2 m specific humidity, precipitation rate, 10 m wind vectors, downward longwave radiation, and net shortwave radiation. For the year 2007-2010, initial salinity and temperature are also adjusted.

Uncertainties for the control variables and observations are the same as in Koldunov et al. (2017). Sea ice thickness uncertainty is provided by Ricker et al. (2017) and is revised based on Xie et al. (2018). Sea ice concentration uncertainties are defined as Fenty and Heimbach (2013).
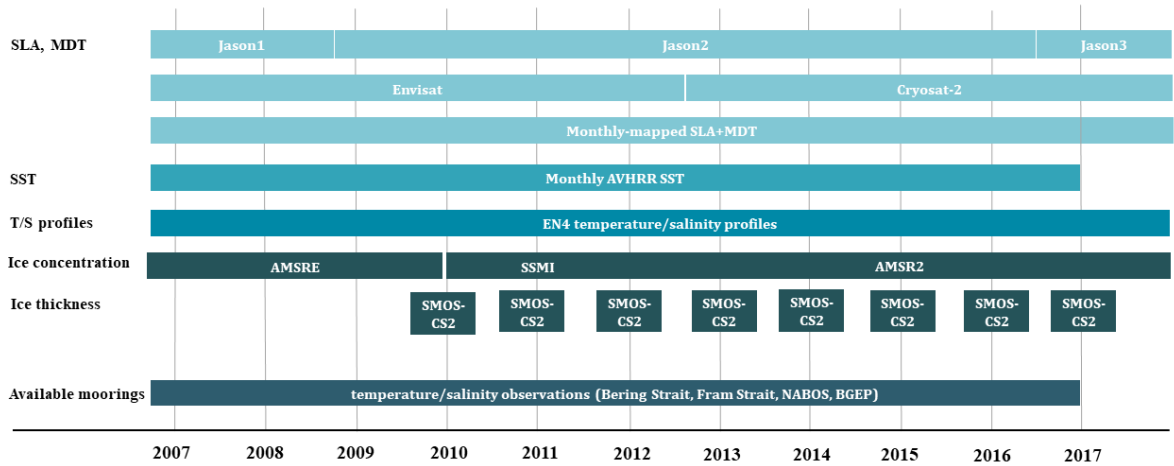
Figure 12. Available observations over the period 2007-2017.

4.2 Evaluation of the optimization

Minimization algorithms based on (Gilbert & Lemaréchal, 2009) is used to reduce the cost function iteratively. Thirteen iterations are performed in the year 2007-2010 and ten iterations are performed in the other two chunks. At the last iteration of each chunk, further reduction of the cost function is tiny.

Figure 13 shows the percentage cost function reduction of total cost and each component in different assimilation chunks. Negative values mean that the model-data difference is increased. The total cost function is reduced by ~28.4%. Most of the individual components are reduced except for SLA, SST within ice edge regions, and monthly mapped SLA over ice cover regions. For sea ice concentration and SST, which are easily changed by atmospheric forcing, error reductions in the three chunks seem homogenous. However, error reduction of mean dynamic topography and mooring observations increase in the latter years. Due to the daily observing frequency and spatial coverage, sea ice concentration dominates the cost function (57.8%) and is significantly improved.
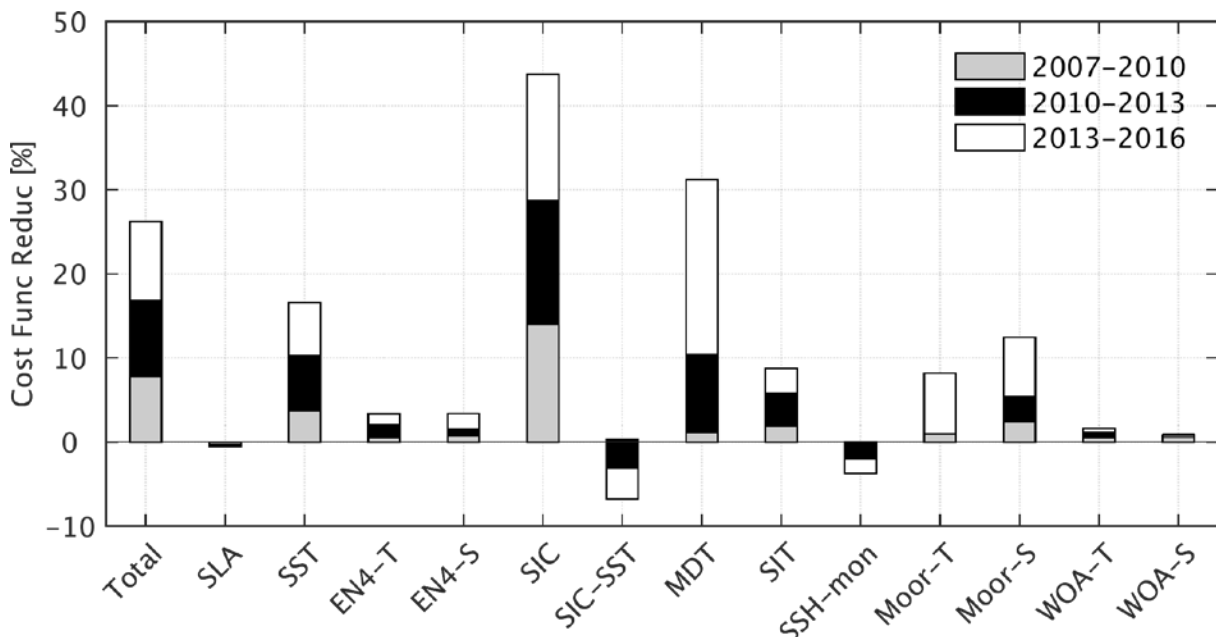

Figure 13. Percentage reduction of the total cost function and individual constitutes in the three chunks (see legend).

4.3 Improvement of the sea ice parameters

Figure 14 displays normalized root mean square errors (RMSEs) for sea ice concentration and sea ice thickness averaged over the entire model domain with and without data assimilation. The normalized RMSEs should be ~1 after the optimization. In the control run, normalize RMSEs of sea ice concentration (the upper panel) range from 1.2-2.4, with more pronounced errors in the summer season. The normalize RMSEs are reduced to ~1.6 in the summer season. In the winter season, the regional-averaged normalized RMSEs are slightly reduced. Over the whole assimilation period, mean normalized RMSEs of sea ice concentration are reduced from 1.6 to 1.2. Normalized RMSEs of ice thickness is also reduced, with the mean error reduced from 1.4 to 1.13. Overall, sea ice thickness and sea ice concentrations match the observations well.
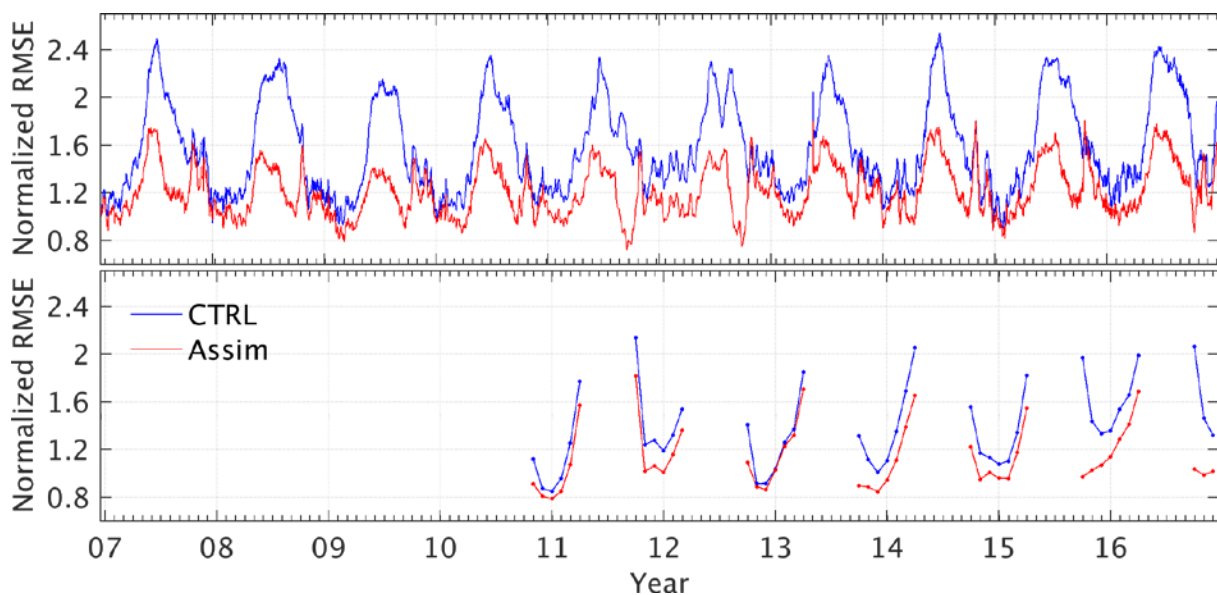
Figure 14. Normalized RMSEs for sea ice concentration (upper panel) and sea ice thickness (bottom panel) in the control run and data assimilation.

Figure 15 shows sea ice concentration errors in the summer season (a,b) and the winter season (c,d) in the control run and after data assimilation. Ice edges (15% ice concentration) from the control run (green dotted line), the data assimilation experiment (blue dotted line), and observations (black dotted line) are overlaid. The control run simulates a much wider ice edge (15% ice concentration) than the observation in both the summer sea and the winter season. After data assimilation, ice edges match the observations well. In the summer season (Figure 15), the control run simulates 20%-30% more ice concentration in Canadian Archipelago, the Beaufort Sea, the Laptev Sea, the Kara Sea, and the Barents Sea and ~20% less ice concentration in the central Arctic Ocean. Sea ice edge extends much farther than observations. Most of these errors are reduced after data assimilation, and the ice edge also matches the observed ice edge very well. Along the coast, there are considerable errors that may result from model deficiency (Fenty & Heimbach, 2013). In the winter season, the control simulates a much wider ice edge and more ice concentration along ice edge regions (Figure 15d). Although averaged normalized RMSEs are small (Figure 14), we still see significant errors over the ice edge regions (Figure 15d) after data assimilation. The errors along the ice edge regions are expected since sea ice processes along the ice edge is more nonlinear than linear (Figure 3), and the adjoint model cannot capture all ice concentration error signals.
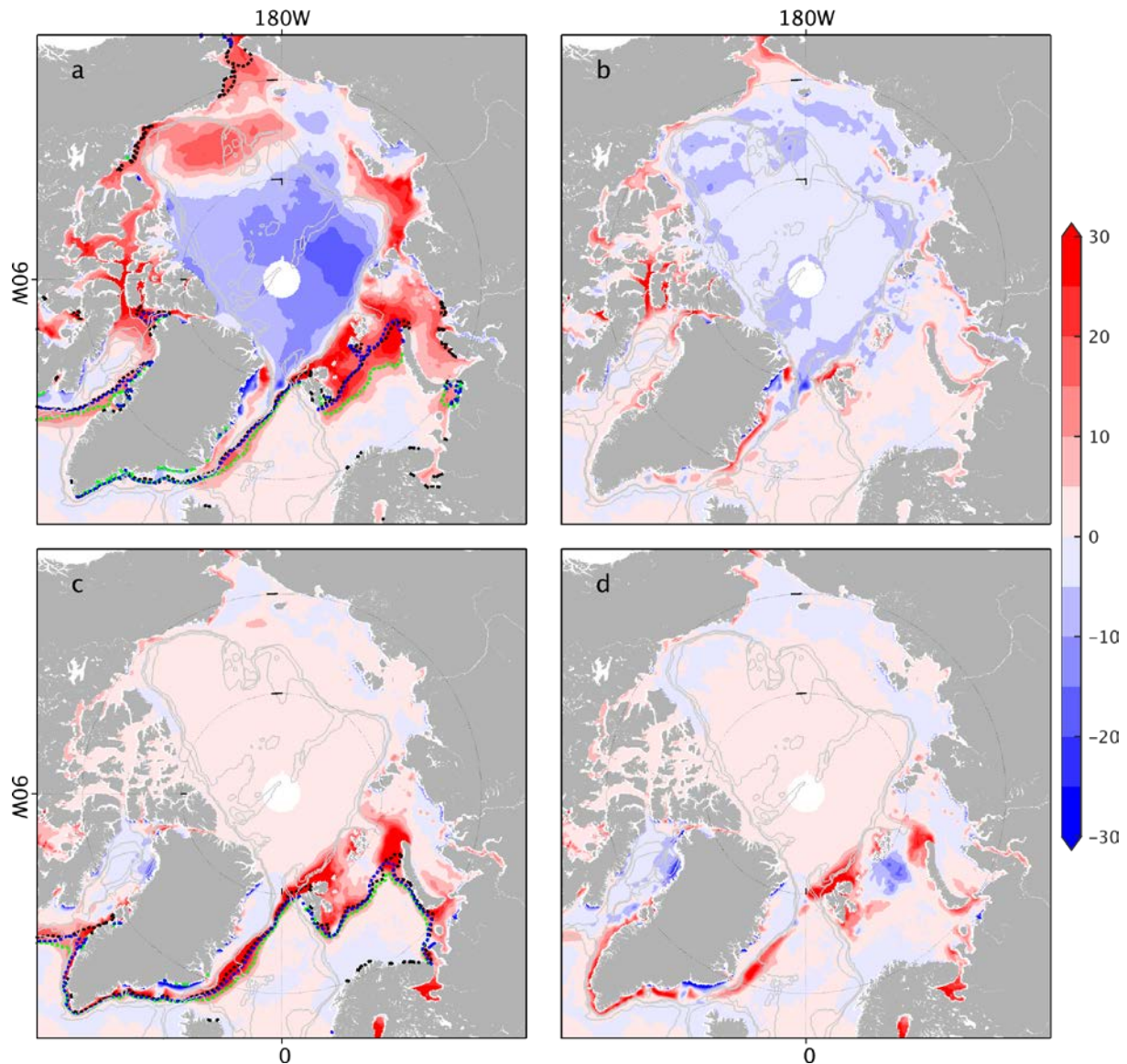
Figure 15. Sea ice concentration error in the summer season in the control run (a) and after data assimilation (b). (c) and (d) are the same as (a) and (b) but in the winter season. Dotted lines in (a) and (c) mark ice edges (15% ice concentration) in the control run (green), after data assimilation (blue), and in the observations(black).

Sea ice thickness observations are only available in the winter season. Sea ice thickness error in the control run (Figure 16a) shows a similar pattern with sea ice concentration error in the summer season (Figure 15a), with less ice north Greenland and CAA and more ice in the surrounding areas. After data assimilation (Figure 16b), both positive and negative errors are reduced in most of the regions. Positive bias in the Beaufort Sea and marginal seas is reduced by -0.1~-0.2 m, and negative bias north of Greenland and CAA is reduced by ~0.2-0.4 m. Figure 16d shows ice thickness increments in the first chunk (2007-2010). Since SMOS-CS2 ice thickness is only available over the last two months of the year 2010 which contributes little to the total cost function, and ice thickness increments pattern matches ice concentration improvement pattern (Figure 15a and b), ice thickness benefits from assimilating ice concentration data. After data assimilation, the remaining errors are considerably large than those in the OSSEs. The significant improvement of sea ice thickness is mainly caused by the adjustment of initial condition (32.8%), 2 m air temperature (34.6%). However, sea ice thickness observations are available almost four years later than the start of data assimilation. And corrections of the initial condition can be small. The

remaining errors may also be related to sea ice model deficiency and need to be further investigated.
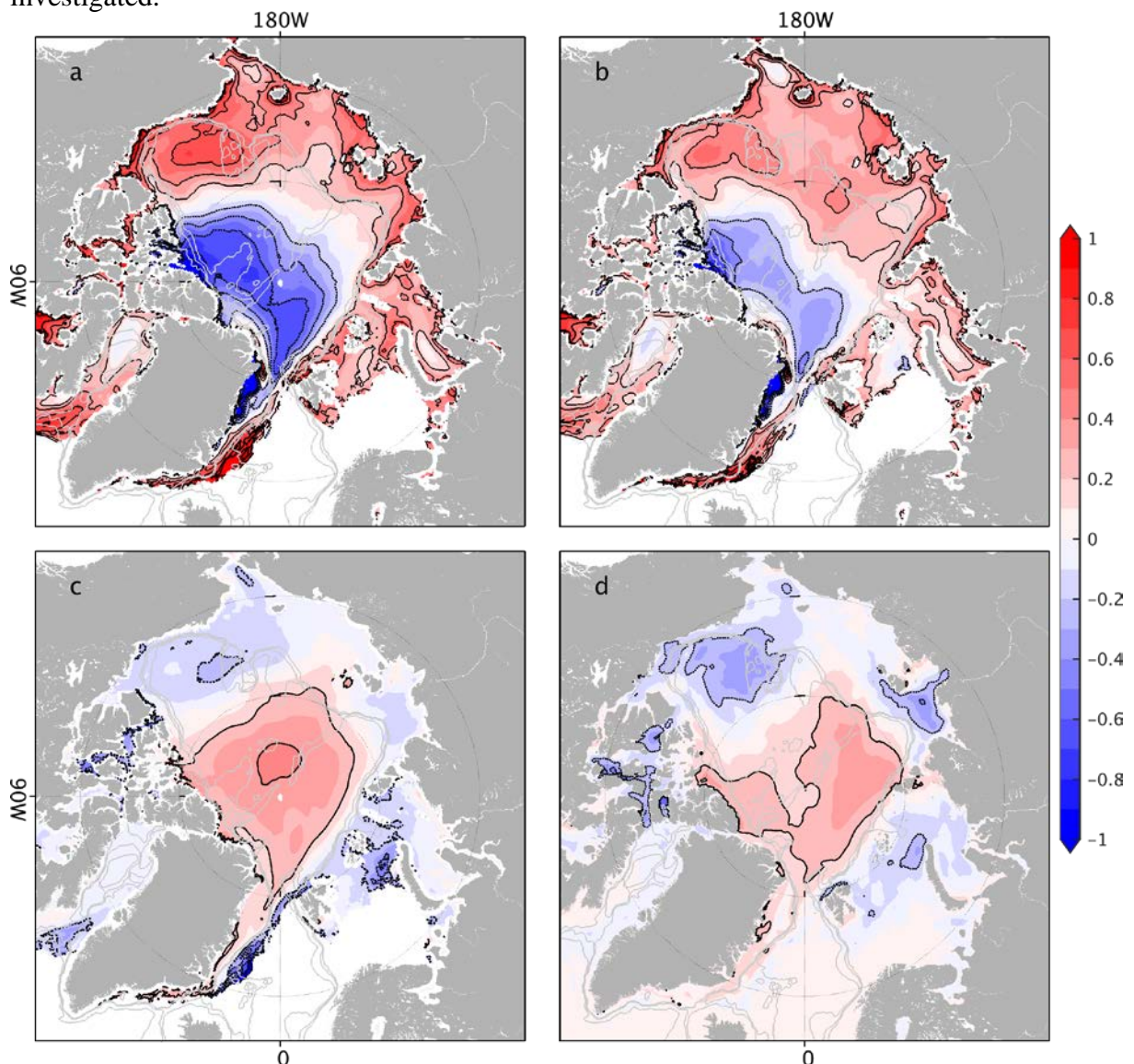

Figure 16. Normalized RMSEs for sea ice concentration (upper panel) and sea ice thickness (bottom panel) in the control run and data assimilation.

4.4 Temperature and Salinity Changes

Changes in ocean temperature are suspected to influence the ice cover (Polyakov et al., 2010). However, in the OSSEs, changes in temperature are mainly as a result of ice changes. Here, we will explore temperature and salinity changes in the synthesis and explain the increments.

Figure 17a and c show temperature difference between the control run and WOA18 over the top 50 m and 50-500 m. Over ice-cover regions, the temperature in the control run is slightly lower the climatology. However, the temperature in GIN seas is much warmer than the climatology, and the warm water is transported to the Arctic Ocean through the Fram Strait and the Barents Sea, resulting in a warm Arctic Atlantic layer. Temperature increments in the top layer (Figure 16b) exist in regions where ice concentration is reduced in the summer season. The temperature changes are probably caused by enhanced air-sea interaction due to reduced ice cover. In the intermediate layer, slightly temperature reduction is visible along the pathway of Atlantic inflow through Franz Josef Land. Compared with the results in OSSEs (Figure 7d), changes related to the mooring in Fram Strait is not apparent. An explanation for

the difference is that the OSSEs assume the moorings observe temperature profiles from 50-1000m while in reality, the moorings usually observe temperature and salinity at no more than three levels. Therefore, mooring observations in the Fram Strait need to be enhanced to capture the Atlantic inflow better.
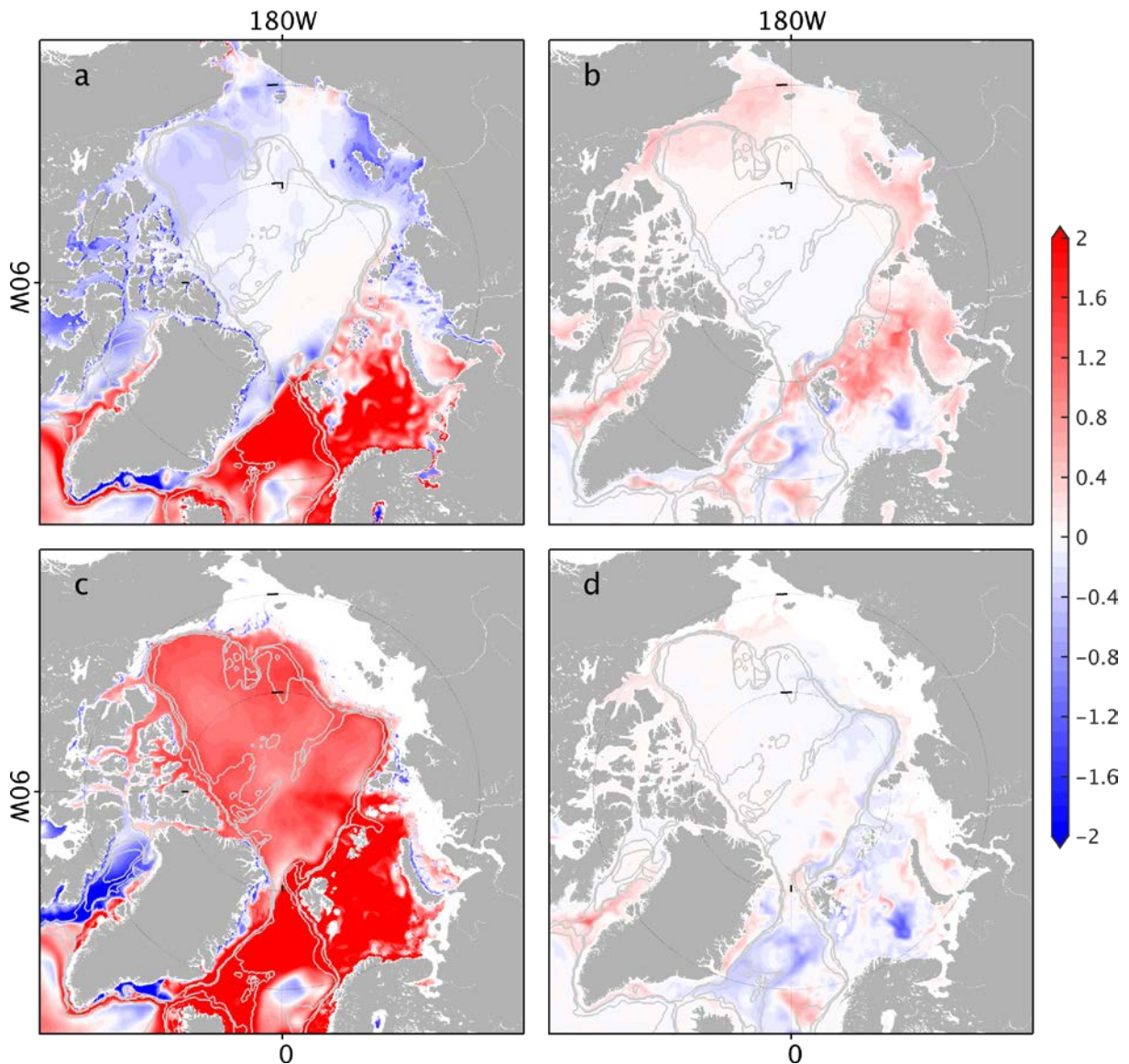
Figure 17. Ocean temperature errors and temperature increments after data assimilation over the upper 50 m (a,b) and between 50-800 m (c,d).

Similar to the temperature changes, salinity changes (Figure 17b) are small compared with the model-data difference (Figure 17a). Changes in salinity are also related to sea ice reduction. Although sea ice is reduced in the Barents Sea, the Laptev Sea, and the Beaufort Sea, we note that salinity is reduced in the Beaufort Sea but is increased in the Barents Sea and the Laptev Sea. The difference may be caused by changes in air-sea interaction with reduced ice caps. On the one hand, sea ice reduction releases freshwater to the ocean and reduce the salinity. On the other hand, it also increases air-sea interaction and may increase evaporation. In our case, both these two processes occur when ice cover is reduced.
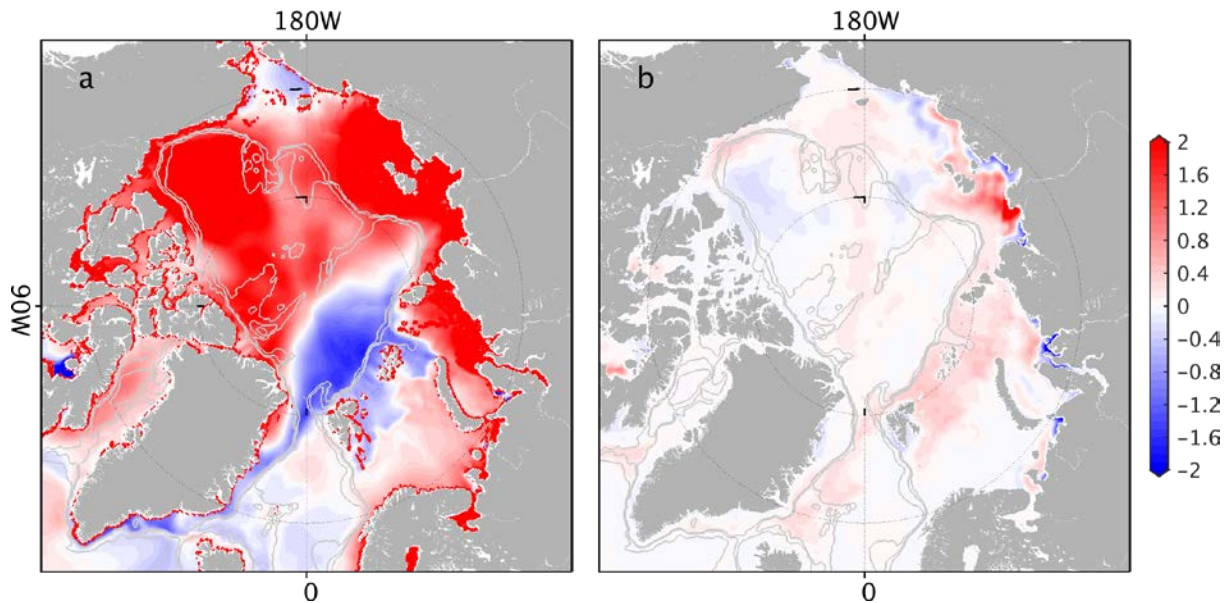
Figure 18. Ocean salinity errors and temperature increments after data assimilation over the top 50 m (a,b).

5.   Summary

In this study, we use a coupled ocean-sea ice model and its adjoint to assimilate observations into the model. We perform OSSEs to evaluate the capacity of the existing Arctic Ocean observing system on monitoring the Arctic Ocean changes. Then, we produced a 10-year ocean synthesis (2007-2016) by assimilating all available observations into our model. In both OSSEs and the 10-year ocean-sea ice synthesis, we see that sea ice concentration contributes most to the total cost function and is improved the most after data assimilation. The improvement benefits from the high spatiotemporal coverage of sea ice concentration observations. Sea ice thickness is also improved. Based on OSSEs (see Table 3), we note that sea ice thickness provides additional information to adjust initial conditions and 2 m air temperature.

Changes in temperature and salinity in the OSSEs and the synthesis show different patterns. In OSSEs, the temperature in the GIN seas is significantly improved, and the additional effect of moorings on the Atlantic inflow is visible. However, in the 10-year synthesis, temperature and salinity changes are mainly in the ice reduction regions due to enhanced air-sea interaction. Changes in the GIN seas are small. Slightly improvement of Atlantic inflow through the Franz Josef Land is visible. There are two possible reasons for the degraded performance in the 10-year reanalysis: 1) moorings have less spatiotemporal coverage in reality than in OSSEs; 2) fewer iterations are performed in the 10-year synthesis, and SST errors are not significantly reduced due to its small contribution to the total cost.

Overall, the assimilation experiments indicate that the dominant mode that can be improved by assimilating all available observations is sea ice processes, especially sea ice concentration variability. Improvement in sea ice concentration is govern by corrections to the wind vectors. The reduction of sea ice cover after data assimilation enhances air-sea interaction and hence changes the temperature and salinity subsequently.

Due to the long memory of Atlantic inflow into the Arctic Ocean, the potential effects of moorings deployed in the Fram Strait and the continental slope of the Laptev Sea are noticeable in the OSSEs. However, the mooring system needs to be enhanced since temperature and salinity are only observed at a couple of levels in reality. Although the numbers of in-situ profiles have increased significantly over the past decades, it is still too sparse, and its effects are not apparent in our data assimilation experiments.

6. References

Armitage, T. W., Bacon, S., Ridout, A. L., Thomas, S. F., Aksenov, Y., & Wingham, D. J. (2016). Arctic sea surface height variability and change from satellite radar altimetry and GRACE, 2003–2014. *Journal of Geophysical Research: Oceans, 121*(6), 4303-4322.

Baumann, T. M., Polyakov, I. V., Pnyushkov, A. V., Rember, R., Ivanov, V. V., Alkire, M. B., . . . Carmack, E. C. (2018). On the Seasonal Cycles Observed at the Continental Slope of the Eastern Eurasian Basin of the Arctic Ocean. *Journal of Physical Oceanography, 48*(7), 1451-1470. doi: 10.1175/jpo-d-17-0163.1

Behrendt, A., Sumata, H., Rabe, B., & Schauer, U. (2018). UDASH – Unified Database for Arctic and Subarctic Hydrography. *Earth Syst. Sci. Data, 10*(2), 1119-1138. doi: 10.5194/essd-10-1119-2018

Casey, K. S. (2010). Cite as: Casey, KS, TB Brandon, P. Cornillon, and R. Evans (2010)." The Past, Present and Future of the AVHRR Pathfinder SST Program", in Oceanography from Space: Revisited, eds. V. Barale, JFR Gower, and L. Alberotanza, Springer.

Comiso, J. C., Parkinson, C. L., Gersten, R., & Stock, L. (2008). Accelerated decline in the Arctic sea ice cover. *Geophysical Research Letters, 35*(1). doi: 10.1029/2007gl031972

Dee, D. P., Uppala, S., Simmons, A., Berrisford, P., Poli, P., Kobayashi, S., . . . Bauer, d. P. (2011). The ERA‐Interim reanalysis: Configuration and performance of the data assimilation system. *Quarterly Journal of the royal meteorological society, 137*(656), 553-597.

Dmitrenko, I. A., Polyakov, I. V., Kirillov, S. A., Timokhov, L. A., Frolov, I. E., Sokolov, V. T., . . . Walsh, D. (2008). Toward a warmer Arctic Ocean: Spreading of the early 21st century Atlantic Water warm anomaly along the Eurasian Basin margins. *Journal of Geophysical Research: Oceans, 113*(C5).

Dukhovskoy, D. S., Johnson, M. A., & Proshutinsky, A. (2004). Arctic decadal variability: An auto-oscillatory system of heat and fresh water exchange. *Geophysical Research Letters, 31*(3). doi: 10.1029/2003gl019023

Errico, R. M., Yang, R., Privé, N. C., Tai, K.-S., Todling, R., Sienkiewicz, M. E., & Guo, J. (2013). Development and validation of observing-system simulation experiments at NASA's Global Modeling and Assimilation Office. *Quarterly Journal of the Royal Meteorological Society, 139*(674), 1162-1178. doi: 10.1002/qj.2027

Fenty, I., & Heimbach, P. (2013). Coupled Sea Ice–Ocean-State Estimation in the Labrador Sea and Baffin Bay. *Journal of Physical Oceanography, 43*(5), 884-904. doi: 10.1175/jpo-d-12-065.1

Giering, R., & Kaminski, T. (1998). Recipes for adjoint code construction. *ACM Transactions on Mathematical Software (TOMS), 24*(4), 437-474.

Gilbert, J. C., & Lemaréchal, C. The module M1QN3.

Giles, K. A., Laxon, S. W., Ridout, A. L., Wingham, D. J., & Bacon, S. (2012). Western Arctic Ocean freshwater storage increased by wind-driven spin-up of the Beaufort Gyre. *Nature Geoscience, 5*, 194. doi: 10.1038/ngeo1379

https://www.nature.com/articles/ngeo1379#supplementary-information

Good, S. A., Martin, M. J., & Rayner, N. A. (2013). EN4: Quality controlled ocean temperature and salinity profiles and monthly objective analyses with uncertainty estimates. *Journal of Geophysical Research: Oceans, 118*(12), 6704-6716. doi: 10.1002/2013jc009067

Hibler III, W. (1979). A Dynamic Thermodynamic Sea Ice Model. *Journal of Physical Oceanography, 9*(4), 815-846. doi: 10.1175/1520-0485(1979)009<0815:adtsim>2.0.co;2

Hibler III, W. (1980). Modeling a Variable Thickness Sea Ice Cover. *Monthly Weather Review, 108*(12), 1943-1973. doi: 10.1175/1520-0493(1980)108<1943:mavtsi>2.0.co;2

Hoteit, I., Cornuelle, B., Köhl, A., & Stammer, D. (2005). Treating strong adjoint sensitivities in tropical eddy-permitting variational data assimilation. *Quarterly Journal of the Royal Meteorological Society, 131*(613), 3659-3682. doi: 10.1256/qj.05.97

Jahn, A., Aksenov, Y., Cuevas, B., Steur, L., Häkkinen, S., Hansen, E., . . . Kauker, F. (2012). Arctic Ocean freshwater: How robust are model simulations? *Journal of Geophysical Research: Oceans, 117*(C8).

Jungclaus, J. H., Haak, H., Latif, M., & Mikolajewicz, U. (2005). Arctic–North Atlantic Interactions and Multidecadal Variability of the Meridional Overturning Circulation. *Journal of Climate, 18*(19), 4013-4031. doi: 10.1175/jcli3462.1

Köhl, A., & Serra, N. (2014). Causes of Decadal Changes of the Freshwater Content in the Arctic Ocean. *Journal of Climate, 27*(9), 3461-3475. doi: 10.1175/jcli-d-13-00389.1

Köhl, A., & Willebrand, J. (2002). An adjoint method for the assimilation of statistical characteristics into eddy‐resolving ocean models. *Tellus A, 54*(4), 406-425.

Kalnay, E., Kanamitsu, M., Kistler, R., Collins, W., Deaven, D., Gandin, L., . . . Woollen, J. (1996). The NCEP/NCAR 40-year reanalysis project. *Bulletin of the American meteorological Society, 77*(3), 437-471.

Koldunov, N. V., Köhl, A., Serra, N., & Stammer, D. (2017). Sea ice assimilation into a coupled ocean–sea ice model using its adjoint. *The Cryosphere, 11*(5), 2265-2281. doi: 10.5194/tc-11-2265-2017

Koldunov, N. V., Köhl, A., & Stammer, D. (2013). Properties of adjoint sea ice sensitivities to atmospheric forcing and implications for the causes of the long term trend of Arctic sea ice. *Climate dynamics, 41*(2), 227-241.

Koldunov, N. V., Serra, N., Köhl, A., Stammer, D., Henry, O., Cazenave, A., . . . Gao, Y. (2014). Multimodel simulations of Arctic Ocean sea surface height variability in the period 1970–2009. *Journal of Geophysical Research: Oceans, 119*(12), 8936-8954.

Kwok, R., & Rothrock, D. A. (2009). Decline in Arctic sea ice thickness from submarine and ICESat records: 1958–2008. *Geophysical Research Letters, 36*(15). doi: 10.1029/2009gl039035

Large, W. G., McWilliams, J. C., & Doney, S. C. (1994). Oceanic vertical mixing: A review and a model with a nonlocal boundary layer parameterization. *Reviews of Geophysics, 32*(4), 363-403.

Losch, M., Menemenlis, D., Campin, J.-M., Heimbach, P., & Hill, C. (2010). On the formulation of sea-ice models. Part 1: Effects of different solver implementations and parameterizations. *Ocean Modelling, 33*(1-2), 129-144.

Mahfouf, J.-F. (1999). Influence of physical processes on the tangent‐linear approximation. *Tellus A, 51*(2), 147-166.

Marshall, J., Adcroft, A., Hill, C., Perelman, L., & Heisey, C. (1997). A finite‐volume, incompressible Navier Stokes model for studies of the ocean on parallel computers. *Journal of Geophysical Research: Oceans, 102*(C3), 5753-5766.

McPhee, M. G., Stanton, T. P., Morison, J. H., & Martinson, D. G. (1998). Freshening of the upper ocean in the Arctic: Is perennial sea ice disappearing? *Geophysical Research Letters, 25*(10), 1729-1732. doi: doi:10.1029/98GL00933

Morison, J., Kwok, R., Peralta-Ferriz, C., Alkire, M., Rigor, I., Andersen, R., & Steele, M. (2012). Changing Arctic Ocean freshwater pathways. *Nature, 481*, 66. doi: 10.1038/nature10705 https://www.nature.com/articles/nature10705#supplementary-information

Morison, J., Wahr, J., Kwok, R., & Peralta‐Ferriz, C. (2007). Recent trends in Arctic Ocean mass distribution revealed by GRACE. *Geophysical Research Letters, 34*(7).

Oke, P. R., & Sakov, P. (2008). Representation Error of Oceanic Observations for Data Assimilation. *Journal of Atmospheric and Oceanic Technology, 25*(6), 1004-1017. doi: 10.1175/2007jtecho558.1

Polyakov, I. V., Timokhov, L. A., Alexeev, V. A., Bacon S., Dmitrenko, I. A., Fortier, L., . . . Toole, J. (2010). Arctic Ocean Warming Contributes to Reduced Polar Ice Cap. *Journal of Physical Oceanography, 40*(12), 2743-2756. doi: 10.1175/2010jpo4339.1

Proshutinsky, A., Aksenov, Y., Kinney, J. C., Gerdes, R., Golubeva, E., Holland, D., . . . Popova, E. (2011). Recent advances in Arctic ocean studies employing models from the Arctic Ocean Model Intercomparison Project. *Oceanography, 24*(3), 102-113.

Proshutinsky, A., Krishfield, R., Timmermans, M.-L., Toole, J., Carmack, E., McLaughlin, F., . . . Shimada, K. (2009). Beaufort Gyre freshwater reservoir: State and variability from observations. *Journal of Geophysical Research: Oceans, 114*(C1). doi: 10.1029/2008jc005104

Proshutinsky, A. Y., & Johnson, M. A. (1997). Two circulation regimes of the wind‐driven Arctic Ocean. *Journal of Geophysical Research: Oceans, 102*(C6), 12493-12514.

Quadfasel, D., SY, A., WELLS, D., & TUNIK, A. (1991). Warming in the Arctic. *Nature, 350*(6317), 385.

Ricker, R., Hendricks, S., Kaleschke, L., Tian-Kunze, X., King, J., & Haas, C. (2017). A weekly Arctic sea-ice thickness data record from merged CryoSat-2 and SMOS satellite data. *The Cryosphere, 11*(4), 1607-1623. doi: 10.5194/tc-11-1607-2017

Rose, S. K., Andersen, O. B., Passaro, M., Ludwigsen, C. A., & Schwatke, C. (2019). Arctic Ocean Sea Level Record from the Complete Radar Altimetry Era: 1991–2018. *Remote Sensing, 11*(14), 1672.

Schauer, U., Beszczynska-Möller, A., Walczowski, W., Fahrbach, E., Piechura, J., & Hansen, E. (2008). Variation of measured heat flow through the Fram Strait between 1997 and 2006 *Arctic–Subarctic Ocean Fluxes* (pp. 65-85): Springer.

Semtner, A. J. (1976). A model for the thermodynamic growth of sea ice in numerical investigations of climate. *Journal of Physical Oceanography, 6*(3), 379-389.

Smith, W. H. F., & Sandwell, D. T. (1997). Global Sea Floor Topography from Satellite Altimetry and Ship Depth Soundings. *Science, 277*(5334), 1956-1962. doi: 10.1126/science.277.5334.1956

Spreen, G., Kaleschke, L., & Heygster, G. (2008). Sea ice remote sensing using AMSR-E 89-GHz channels. *Journal of Geophysical Research: Oceans, 113*(C2). doi: 10.1029/2005jc003384

Sugiura, N., Masuda, S., Fujii, Y., Kamachi, M., Ishikawa, Y., & Awaji, T. (2015). A framework for interpreting regularized state estimation. *arXiv preprint arXiv:1511.04790.*

Uotila, P., Goosse, H., Haines, K., Chevallier, M., Barthélemy, A., Bricaud, C., . . . Zhang, Z. (2019). An assessment of ten ocean reanalyses in the polar regions. *Climate Dynamics, 52*(3), 1613-1650. doi: 10.1007/s00382-018-4242-z

Woodgate, R. A., Weingartner, T. J., & Lindsay, R. (2012). Observed increases in Bering Strait oceanic fluxes from the Pacific to the Arctic from 2001 to 2011 and their impacts on the Arctic Ocean water column. *Geophysical Research Letters, 39*(24).

Xie, J., Bertino, L., Counillon, F., Lisæter, K. A., & Sakov, P. (2017). Quality assessment of the TOPAZ4 reanalysis in the Arctic over the period 1991–2013. *Ocean Sci., 13*(1), 123-144. doi: 10.5194/os-13-123-2017

Xie, J., Counillon, F., & Bertino, L. (2018). Impact of assimilating a merged sea-ice thickness from CryoSat-2 and SMOS in the Arctic reanalysis. *The Cryosphere, 12*(11), 3671-3691. doi: 10.5194/tc-12-3671-2018

Zhang, J., & Hibler III, W. (1997). On an efficient numerical method for modeling sea ice dynamics. *Journal of Geophysical Research: Oceans, 102*(C4), 8691-8702.

Zhang, J., & Steele, M. (2007). Effect of vertical mixing on the Atlantic Water layer circulation in the Arctic Ocean. *Journal of Geophysical Research: Oceans, 112*(C4).

Zhu, J., Wang, H., & Masafumi, K. (2002). The improvement made by a modified TLM in 4DVAR with a geophysical boundary layer model. *Advances in Atmospheric Sciences, 19*(4), 563-582.

----------- END of DOCUMENT-----------

INTAROS

This report is made under the project
Integrated Arctic Observation System (INTAROS)
funded by the European Commission Horizon 2020 program
Grant Agreement no. 727890.

Project partners: